LBL-28480
Preprint

# Lawrence Berkeley Laboratory
UNIVERSITY OF CALIFORNIA

To be published in Physical Review C

## Changes in Target Fragmentation Mechanisms with Increasing Projectile Energy in Intermediate Energy Nuclear Collisions

W. Loveland, K. Aleklett, L. Sihver, Z. Xu, C. Casey, D.J. Morrissey,
J.O. Liljenzin, M. de Saint-Simon, and G.T. Seaborg

January 1990

NUCLEAR SCIENCE DIVISION

LOAN COPY
Circulates
for 2 weeks
LBL-28480
Copy 2
Bldg. 50 Library.

Prepared for the U.S. Department of Energy under Contract Number DE-AC03-76SF00098.

## DISCLAIMER

This document was prepared as an account of work sponsored by the United States Government. While this document is believed to contain correct information, neither the United States Government nor any agency thereof, nor the Regents of the University of California, nor any of their employees, makes any warranty, express or implied, or assumes any legal responsibility for the accuracy, completeness, or usefulness of any information, apparatus, product, or process disclosed, or represents that its use would not infringe privately owned rights. Reference herein to any specific commercial product, process, or service by its trade name, trademark, manufacturer, or otherwise, does not necessarily constitute or imply its endorsement, recommendation, or favoring by the United States Government or any agency thereof, or the Regents of the University of California. The views and opinions of authors expressed herein do not necessarily state or reflect those of the United States Government or any agency thereof or the Regents of the University of California.

LBL 28480

# CHANGES IN TARGET FRAGMENTATION MECHANISMS WITH INCREASING PROJECTILE ENERGY IN INTERMEDIATE ENERGY NUCLEAR COLLISIONS

W. Loveland[a], K. Aleklett[b], L. Sihver[b], Z. Xu[a], C. Casey[a], D.J. Morrissey[c], J.O. Liljenzin[d], M. de Saint-Simon[e], and G.T. Seaborg[f]

Chemistry Dept., Oregon State University, Corvallis, OR 97331[a]

Studsvik Neutron Research Laboratory, S-61182, Nyköping, Sweden[b]

NSCL, Michigan State University, E. Lansing, MI 48824 [c]

Department of Chemistry, University of Oslo, Oslo, Norway[d]

Laboratoire Rene Bernas, F-91406, Orsay, France[e]

Lawrence Berkeley Laboratory, Berkeley, CA 94720, USA[f]

Nuclear Science Division
Lawrence Berkeley Laboratory
University of California
Berkeley, CA 94720

January 1990

This work was supported in part by the Director, Office of Energy Research, Division of Nuclear Physics of the Office of High Energy and Nuclear Physics of the U.S. Department of Energy under Contract No. DE-AM06-76RL02227, and DE-AC03-76SF00098, Task Agreement No. DE-AT06-76ER70035, and the Swedish Natural Science Research Council.

# CHANGES IN TARGET FRAGMENTATION MECHANISMS WITH INCREASING PROJECTILE ENERGY IN INTERMEDIATE ENERGY NUCLEAR COLLISIONS

W. Loveland[(a)], K. Aleklett[(b)], L. Sihver[(b)], Z. Xu[(a)],
C. Casey[(a)], D.J. Morrissey[(c)], J.O. Liljenzin[(d)],
M. de Saint-Simon[(e)], and G.T. Seaborg[(f)]

[(a)]Chemistry Dept., Oregon State University, Corvallis, OR 97331
[(b)]Studsvik Neutron Research Laboratory,S-61182, Nyköping, Sweden
[(c)]NSCL, Michigan State University, E. Lansing, MI 48824
[(d)]Dept. of Chemistry, University of Oslo, Oslo, Norway
[(e)]Laboratoire Rene Bernas, F-91406 Orsay, France
[(f)]Lawrence Berkeley Laboratory, Berkeley, CA 94720

## ABSTRACT

We have measured the target fragment production cross sections and angular distributions for the interaction of 16 MeV/nucleon $^{32}S$, 32 MeV/nucleon $^{40}Ar$ and 44 MeV/nucleon $^{40}Ar$ with $^{197}Au$. We have deduced the fragment isobaric yield distributions and moving frame angular distributions from these data. The fission cross sections decrease with increasing projectile energy and the heavy residue cross sections (which are much larger than previous counter measurements) increase. There is an

unusual change in the fragment isobaric yield distributions in the reactions induced by 32 MeV/N $^{40}$Ar and 44 MeV/N $^{40}$Ar. We have used the symmetry properties of the moving frame distributions to show the relative time scale of the reaction mechanisms involved. The fission fragments associated with the peripheral collision peak in the folding angle distribution originate in a normal, slow fission process in which statistical equilibrium has been established. At the two lowest projectile energies, the fission fragments associated with the central collision peak in the folding angle distribution originate in part in fast, non-equilibrium processes. At the highest projectile energies, there are no fission fragments associated with high momentum transfer events. The intermediate mass fragments originate primarily in events in which statistical equilibrium has not been established.

PACS Numbers 25.70.Np

## I. Introduction

Studies of intermediate energy nuclear collisions are interesting because of the "transitional" character of the intermediate energy regime. In low energy nuclear collisions, the behavior of the colliding nuclei is determined by their mean field while in high energy nuclear collisions, it is the collision of individual nucleons in the nuclei that determines the outcome of the reaction. The intermediate energy regime (projectile energies of 10 to 100 MeV/nucleon) allows one to study how nuclear reaction mechanisms change between these two extreme types of nuclear behavior.

The study of intermediate energy nuclear collisions has many aspects. In this discussion, we shall focus our attention on the experimental characterization of the

fragments of the heavy target nucleus produced in such collisions. These fragments may be roughly classified by mass number, i.e., the intermediate mass fragments ($A_{frag} < A_{target}/3$); the heavy residues ($A_{frag} > 2/3\ A_{target}$) and the fission fragments ($A_{target}/3 < A_{frag} < 2\ A_{target}/3$). It is of interest to see how the mechanism(s) for the production of these fragments change with increasing projectile energy (with constant projectile size.) The recent availability of heavier projectiles such as S, Ar, Kr, etc. makes it possible to study reactions in which large amounts of energy (approaching the total nuclear binding energy) can be transferred from the projectile to the target nucleus.

Interest in this area has been quite high, judging from the large number of survey papers and original contributions[1-31] that have appeared recently. From these many investigations, certain general features of the production of the target fragments have been discerned. They are:

1. The heavy residue production cross sections represent a significant fraction of the total reaction cross section.[5,7,12,23,24,27,29] The heavy residues are produced mostly in peripheral collisions at the higher projectile energies (35 and 44 MeV/nucleon).[18,23,30] Some residues at higher energies result from more central collisions as do most residues at lower projectile energies[23,30] where they can be characterized as evaporation residues.[27] The heavy residue angular distributions are strongly forward-peaked in all cases.[23,24,27] Their velocities range from very low (at the higher projectile energies where detector thresholds preclude observation of some residues[24,27]) to velocities exceeding that of the center of mass (indicating the existence of large nuclear excitation energies). Most of these fragments are produced in incomplete fusion reactions[11,12,18,23,30,31] although some are produced in nearly complete fusion events.[23,30]

2. The intermediate mass fragment production cross sections are substantially lower than those of the heavy residues. They are predominantly produced with a multiplicity of unity in binary events that also yield a heavy residue.[3,14,17,25,26] The reactions producing them involve both non-equilibrated and equilibrated sources with the former being more important (in reactions induced by carbon projectiles).[17,32,33] Incomplete fusion with substantial pre-equilibrium particle emission is the dominant production mechanism.[14,17,26]

3. The fission fragments represent those primary heavy residue reaction products that deexcited by fission rather than particle emission.[12,24,27] They can also represent the result of a special nuclear reaction mechanism, fast fission.[3,6,10,28] In the former case, $\sigma_{HR}/\sigma_{fission}$ increases with increasing projectile energy due to two effects (a) the increasing probability of incomplete fusion, leading to lower mass and atomic numbers of the product nuclei, thus decreasing their fissionability and (b) the faster time scale of the more energetic reactions favors the intrinsically faster process of particle emission vs. the slower collective motion of fission.[27] Whether fission selects the high momentum transfer events relative to those of lower momentum transfer appears to be a complicated feature of the de-excitation of a given set of nuclei.

4. There is a remarkable change in the fragment production mechanism(s) as the projectile energy increases from 27 to 44 MeV/nucleon.[2,8,9,21,23,24,29,30] At projectile energies of 27 MeV/nucleon or below, both central and peripheral collisions result in the production of heavy residues and fission fragments. As the projectile energy is raised to 35 MeV/nucleon, the central collision "peak" in the heavy residue spectra and the fission fragment folding angle distribution disappears although there is a "tail" of

high momentum transfer events. At 44 MeV/nucleon, there are few events corresponding to large momentum transfer. Detailed analyses show the cross section for fusion-like events with large momentum transfer becomes very small at energies of 35-50 MeV/nucleon. The vanishing of such processes is thought to be related to the existence of a maximum temperature or excitation energy of a nucleus.[1,4,9,13,14,15,17,20,21]

Several studies have focussed on the reaction of $^{32}S$ or $^{40}Ar$ with $^{197}Au$.[5,7,8,9,10,13,18,22,23,24,27,29] The cross sections for the formation of heavy residues, fission fragments and intermediate mass fragments have been measured for several projectile energies from 19 to 60 MeV/nucleon.

Measurements of the heavy residues have suffered from detector thresholds of ~0.5 cm/ns which may have biased the results.[24,27]

In this paper, we present the results of single particle inclusive measurements of the yields and angular distributions of the target fragments produced in the interaction of 16 MeV/nucleon $^{32}S$, 32 MeV/nucleon $^{40}Ar$ and 44 MeV/nucleon $^{40}Ar$ with $^{197}Au$. These measurements were made using radiochemical techniques which have superior mass resolution and no detector cutoffs for the heavy residues. The measurements complement and extend the data discussed above.

## II. Experimental Techniques

The measurements described herein were carried out using the facilities of three different accelerators, the LBL 88" cyclotron (16 MeV/nucleon $^{32}S$), the National Superconducting Cyclotron (K500) at MSU (32 MeV/nucleon $^{40}Ar$) and the GANIL accelerator complex (44 MeV/nucleon $^{40}Ar$). The experimental procedures used at each

accelerator were similar with measurements of target fragment formation cross sections and angular distributions being made using radiochemical techniques. The measurement of the fragment angular distributions was made using techniques that have been described previously.[32,33] The reader is referred to Ref. 32 for discussions of the angular resolution of the measurements and the influence of fragment scattering upon the results. The measurements of the target fragment production cross sections at LBL and MSU were made by a simple irradiation of a thick gold foil surrounded by ~15 mg/cm$^2$ carbon catcher foils. The radionuclide content of the irradiated foil stack was determined by off-line gamma ray spectroscopy. Production cross sections were calculated from end of bombardment radionuclide activities.[34] (For the GANIL irradiation, the total nuclide production cross sections were determined by integrating the measured fragment angular distributions.) The detailed irradiation conditions employed at each accelerator are summarized in Table I. (At LBL, two separate irradiations were performed for the cross section measurement to optimize the yields of short and long-lived activities, respectively).

## III. Experimental Results

For the reactions of 16 A MeV $^{32}$S with $^{197}$Au, the angular distributions of 49 different target fragments were measured along with the production cross sections for 95 different radionuclides. For the reaction of 32 A MeV $^{40}$Ar with $^{197}$Au, angular distributions were measured for 40 fragments while the yields of 72 fragments were measured. In the reaction of 44 A MeV $^{40}$Ar with $^{197}$Au, the angular distributions and yields of 72 different target fragments were measured.

A. Target Fragment Yields

The measured target fragment production cross sections are shown in Table II. We have taken a conservative approach in this tabulation and have eliminated from the tables all references to nuclides whose atomic and mass numbers are such that they could possibly be degraded projectile fragments. It is interesting to compare the nuclidic production cross sections measured in this work with that of Hubert et al.[5] who also studied the residue yields in the interaction of 44 MeV/nucleon $^{40}$Ar with heavy targets, including $^{197}$Au. Hubert et al. measured the cross sections and recoil properties of the alpha particle emitting rare earth isotones with N=84-85. We find the products detected in our study to be neutron-deficient as does Hubert et al., but as might be expected, since we do not restrict attention to a specific set of alpha-emitting isotones, we find the maximum residue yields to be much closer to beta stability. (Typical maximum cross sections are observed for nuclei that are ~3 neutrons deficient from beta-stability compared to the 10 neutrons away from stability observed in ref. 5.) The magnitudes of the residue cross sections observed in this work are typically a factor of 2-3 higher than the nuclides observed in ref. 5 and presumably represent a more unbiased sample of heavy residues. We also observe substantial yields of products close to the target nucleus which could not be detected in the work of ref. 5.

A hint of some of the changes that occur in reaction mechanism(s) can be obtained by comparing the ratios of the cross sections of "independent yield" radionuclides from the lowest and highest projectile energies. The ratio of $\sigma$(44 A MeV)/$\sigma$(16 A MeV) has the values of 2.7 $\pm$ 0.2, 1.2 $\pm$ 0.1, 0.65 $\pm$ 0.03, 0.61 $\pm$ 0.03 and 1.72 $\pm$ 0.1 for the nuclides $^{42}$K, $^{48}$Sc,$^{74}$As, $^{84}$Rb,and $^{194}$Au, respectively. One notes in the

values of these ratios evidence for the enhanced production of intermediate mass fragments (K,Sc) as the projectile energy increases, as one might expect from the high production thresholds for these fragments. Fission is inhibited at the higher projectile energy relative to the lower one (for the reasons discussed earlier), leading to decreased production of $^{74}$As and $^{84}$Rb, typical fission products. The yield of the heavy residues, such as $^{194}$Au, is enhanced at the higher projectile energies.

Comparisons of the formation cross sections for common, independent yield fragments from various reactions utilize only a fraction of the available experimental data for each target-projectile system. To more fully utilize the available data, we have deduced mass-yield (isobaric yield) distributions from the measured formation cross sections. The method employed in this estimation procedure has been discussed previously.[35]

The measured nuclidic formation cross sections were placed in ten or twelve groups according to mass number. These cross sections were corrected for precursor beta or alpha decay, where necessary, by assuming that the independent yield cross sections for a given species, $\sigma(Z,A)$, can be expressed as a function of the isobaric yield, $\sigma(A)$ as

$$\sigma(Z,A) = \sigma(A)[2\pi C_Z^2(A)]^{-1/2}\exp[-(Z-Z_{mp})^2/2C_Z^2(A)] \qquad (1)$$

where $C_Z(A)$ is the Gaussian width parameter for mass number A and $Z_{mp}(A)$ is the most probable atomic number for that A. Using this assumption and the further assumption that $\sigma(A)$ varies slowly and smoothly as a function of A (allowing data from

adjacent isobars to be combined in determining $Z_{mp}(A)$ and $C_Z(A)$), one can use the laws of radioactive decay to iteratively correct the measured cumulative formation cross sections for precursor decay.

Within each of the groups, the data were fit to a Gaussian-shaped independent yield distribution. (Only nuclides with well-characterized beta or alpha-decay precursors and well understood members of an isomeric pair were included in the analysis). The nuclidic groupings along with the centers and widths of the Gaussian distributions are given in Table III. The independent yield distributions deduced from the measured formation cross sections are shown in Figures 1, 2, and 3.

If one examines the $Z_{mp}$ functions in Table III, one will find that $Z_{mp}$ generally varies slowly and smoothly with the fragment mass number A. An exception to this occurs for all systems studied for A = 130-150 where there is a discontinuity in the $Z_{mp}$ function. For A > 140, the values of $Z_{mp}$ are ~1 Z unit greater (more neutron deficient) than for A < 140. This effect is seen in many $Z_{mp}$ functions deduced from radioanalytical studies of fragment isobaric yield distributions for reactions involving Au targets.[35,36,37,38] The origins of this effect are not known although one should note that there is a corresponding sharp bend in the valley of beta stability at this point. Other possible effects could involve unknown aspects of nuclear decay schemes in this region where alpha and beta feeding are important, the possibility of double-humped charge distributions, etc. Detailed radiochemical studies of charge distributions in this region would be of interest. Not having these detailed measurements, we chose to treat all deduced isobaric yields in this mass region (A = 130-150) as being uncertain. We have made smooth extrapolations through the deduced isobaric yield data due to this

uncertainty.

The isobaric yield distributions obtained from integration of the independent yield distributions are shown in Figure 4. The individual distributions are shown with solid curves drawn to guide the eye through the data. The individual distributions are compared also in Figure 4. The error bars on the integrated data points reflect only the uncertainties due to counting statistics and do not take into account any uncertainties due to lack of knowledge of the absolute beam intensity (estimated to be ~10%), or those introduced in the charge distribution curve fitting process. Morrissey et al.[35] have suggested that individual isobaric yields may have systematic uncertainties, due to the fitting process, of ~25%. The uncertainties in the isobaric yields are dominated by the latter source of error, with the typical uncertainty be ~30%.

In the isobaric yield distribution from the reaction of 16 MeV/nucleon $^{32}S$ with $^{197}Au$, one sees relatively small yields of the heavy residues ($\sigma_{HR}$ = ~1365 mb). The most striking feature of the distribution is the large central bump in the yield distribution (going from A=50 to A=170) which is presumably due to the occurrence of fission. The width of this distribution is very large especially when compared to reactions induced by lighter ions of roughly equivalent velocity or kinetic energy. It may suggest the occurrence of fast fission (see Section IV). The centroid of the distribution is near A=100 suggesting the fission of a goldlike object but the breadth of the distribution is such as to also encompass the possibility of complete fusion occurring. (The complete fusion cross section has been estimated[39] to be 510 mb with a total reaction cross section of 3565 mb.) The cross section associated with the central bump is estimated to be 2300 mb, assuming a multiplicity of two for all fragments in this

bump.

The isobaric yield distribution for the 32 MeV/nucleon $^{40}Ar$ + $^{197}Au$ reaction is different than the distribution from the 16 MeV/nucleon $^{32}S$ + $^{197}Au$ reaction. The yield of the heavy residues (A=170-192) has increased substantially ($\sigma_{HR}$ = 1900 mb) while the fission distribution has become narrower and the centroid has shifted to lower mass numbers. The cross section associated with this bump (A=60-120) has decreased ($\sigma_f$ = 1820 mb). The value of the heavy residue cross section measured in this work can be compared with the lower limit for this quantity measured[24] for the interaction of 35 MeV/nucleon $^{40}Ar$ with $^{197}Au$ (using counter techniques) of 315$\pm$80 mb. As recognized by the authors of ref. 24, their measurement represents a lower limit because of an experimental cutoff in their velocity spectra of 0.5 cm/ns. What is notable is the fraction of the heavy residue cross section that apparently lies below this velocity cutoff which amounts to an energy of ~130 keV/nucleon for A=190 fragment. Counter experiments to look at heavy residues need to have lower thresholds than this if they are to measure a representative sample of the heavy residue events which include substantial numbers of very peripheral collisions. There is a discrepancy between the measured value of the fission cross section in this work ($\sigma_f$ = 1820 mb) (and also by implication the work of Jacquet et al.[9] who measured that $\sigma_f$ = 1500-2250 mb for the reaction of 27 MeV/nucleon $^{40}Ar$ with $^{197}Au$) and that of Bizard et al.[24] who deduce that $\sigma_f$ = 800$\pm$140 mb. Bizard et al. measured the folding angle distribution of fission fragments and assumed a 1/sinθ angular distribution for the fission fragments (see below) to derive their value for $\sigma_f$. The changes in the measured isobaric distributions for the two lowest projectile energies are consistent with the data summarized in Section I. As shown

previously, the ratio of $\sigma_{HR}/\sigma_f$ fission increases with increasing projectile energy.

The measured isobaric distribution for the highest projectile energy studied in this work differs significantly from the distribution for the two lower projectile energies. The fission bump in the yield distribution has decreased further in magnitude ($\sigma_f$ = 940 mb) while the yield of the heavy residues has increased further ($\sigma_{HR}$ = 3140 mb). As commented upon previously, the heavy residue production cross section is substantially greater than the value of 800 mb observed in ref. 5. The large change in shape of the distribution for 44 MeV/N $^{40}$Ar + $^{197}$Au compared to the lower energy distributions is consistent with the changes in independent nuclide yields discussed previously. It is also consistent with previous studies (discussed in Section I) that suggest a large change in fragment production mechanisms in reactions induced by 32 MeV/N $^{40}$Ar and 43 MeV/N $^{40}$Ar. The disappearance of fission events associated with the "central collision" peak in folding angle distributions (large $\eta_I$) is apparently mirrored by the disappearance of the high A members of the fission yield distribution (which have large $\eta_I$ values).

The excitation functions for fission and heavy residue production are shown in Figure 5. For the $^{40}$Ar + $^{197}$Au reaction, as previously shown for the $^{12}$C + $^{197}$Au reaction,[40] the probability that the primary target-like residue will deexcite by fission decreases with increasing projectile energy. If we assume that $\sigma_f + \sigma_{HR}$ is a measure of the incomplete fusion cross section, we may compare our data to a recent calculation[41] of this quantity for the Ar + Au reaction (Fig. 5). The calculation significantly underestimates the measured values of $\sigma_f + \sigma_{HR}$ at the higher energies. This may be due to the exclusion in the model of ref. 41 of events having very large impact

parameters. (In the model of ref. 41, incomplete fusion can occur only for impact parameters less than some critical value, $b_{cr}$). Alternatively, our data may include "spallation-like" events which would not be simulated by a classical trajectory calculation wherein $b_{cr}$ is estimated from these trajectories which are captured in the pocket of the interaction potential.

B. Fragment Angular Distributions

Tables of the 161 measured fragment angular distributions are available upon request from one of the authors (KA). A representative set of the individual fragment angular distributions for each reaction is shown in Figures 6, 7, 8, and 9. The near target residues ($^{194}$Au,$^{196}$Au, and $^{198}$Au) have the characteristic sidewise-peaked angular distributions of the heavy products of quasi-elastic scattering (Fig. 6). Note that $^{192}$Au (and lighter fragments) are apparently not produced by this reaction mechanism. A more detailed analysis of these interesting reactions is presented elsewhere.[42] However, it is worth noting that the appropriate target fragment production cross sections agree fairly well with the systematics of quasi-elastic one neutron transfer reactions.[43] These systematics predict that the angle-integrated quasielastic one-neutron-transfer cross section $\sigma$, when multiplied by $(B_i \cdot B_f)^{1.1}$ have a simple functional dependence upon $Q_{gg}$. $B_i$ and $B_f$ are the neutron binding energies in the donor and acceptor nuclei, respectively, and $Q_{gg}$ is the ground state Q value. For the reactions $^{197}$Au($^{32}$S,$^{33}$S)$^{196}$Au, $^{197}$Au($^{32}$S,$^{31}$S)$^{198}$Au, and the $^{197}$Au($^{40}$Ar,$^{41}$Ar)$^{196}$Au, the systematics[43] predict cross sections of 187, 5.5 and 144 mb. The appropriate measured values are 116 $\pm$ 12, 4.3 $\pm$ 0.3 and 150 $\pm$ 40 mb, respectively.

In the reaction of 16 MeV/nucleon $^{32}S$ with $^{197}Au$, the fragments with A=55-170 are part of a large central bump in the isobaric yield distribution that has the characteristic shape of a fission mass yield distribution. When one examines the fragment angular distributions for this reaction (Figure 7), one sees that the fragments with A=46-103 have a similar "dipper" shape while the heavier members of this peak in the mass distribution (A=121-169) have a very different shape, suggesting a difference in production mechanisms. The latter group of fragments exhibits a much more forward-peaked distribution similar to that observed for the heavy residues whose distribution is strongly forward-peaked as expected.

For the interaction of 32 MeV/nucleon $^{40}Ar$ with $^{197}Au$, the central fission peak in the mass distribution extends from about A=60 to A=130. The intermediate mass fragments (A<60) show strongly forward-peaked angular distributions while the members of the lower half of the central fission peak in the mass distribution also have forward-peaked distributions and similar "dipper" shapes (Fig. 8). As in the reaction of 16 MeV/nucleon $^{32}S$ with $^{197}Au$, the high mass number members of this central peak (A=121-131) have very forward-peaked distributions of a different shape. One also notes the more forward-peaked distribution of the neutron-deficient fission fragments (such as $^{97}Ru$) compared to the neutron-rich fragments (such as $^{103}Ru$). This effect is well known in high energy reactions. It can be shown[33] that the n-rich and n-poor fragments result from a single mechanism, fission, that occurs after varying amounts of energy and momentum are deposited in the target nucleus in the initial projectile-target encounter. The differential cross sections for heavy residue (A>150) production fall off exponentially with increasing angle. While it is difficult to know how to compare

properly the angular distribution for "heavy residues" (measured with a lower velocity cutoff of 0.5 cm/ns)[24] to our data, one can see a general similarity in the shapes of that distribution and the ones measured in this work.

Our data for the reaction of 44 MeV/nucleon $^{40}Ar$ with $^{197}Au$ would indicate a reduced magnitude and width of the fission peak (A=60-110) in the mass distribution. The low mass number members of the fission peak (and the n-rich members) show the dipper-shaped distribution seen at the other energies while the high mass number nuclides show a more forward-peaked distribution. The heavy residue angular distributions show quasi-exponential falloff with increasing angle similar to that seen[36] in the reaction of 19.2 MeV/nucleon $^{16}O$ and 35 MeV/nucleon $^{12}C$ with $^{154}Sm$ where it was shown that a major portion of the width of the angular distributions is due to the effects of particle emission.

In Figure 10, the representative fragment angular distributions from the three reactions are compared. Fragments which are part of the central fission peak in the mass distribution in all systems have similar distributions. The intermediate mass fragments show strongly forward-peaked distributions at the two higher projectile energies where they originate in a process other than fission. The heavy residue distributions are all strongly forward-peaked at all projectile energies and show similar slopes at the two highest projectile energies consistent with the idea of reaching a constant excitation energy limit in the fragmenting system. (If the width of these distributions is due primarily to particle emission,[36] then similar distributions shapes imply similar amounts of particle emission and similar excitation energies and temperatures of the emitting systems.)

Each fragment angular distribution was integrated from 0 to $\pi/2$ and $\pi/2$ to $\pi$ to obtain the ratio of fragments recoiling forward (F) from the target to those recoiling backward (B). To extract further information from the data, the laboratory system angular distributions were transformed into the moving frame of the target residue following the initial target-projectile encounter. To do this, we have assumed that the final velocity of the fragment in the laboratory system can be written as $V_{lab} = V + v$, where the velocity v is the velocity of the moving frame and V is the velocity kick given the target fragment by particle emission or fission at an angle $\theta_{MF}$ with respect to the beam direction in the moving frame. The vector v has components of $v_{\parallel}$ and $v_{\perp}$, parallel and perpendicular to the beam direction. As a first approximation for $\eta_{\parallel}(=v_{\parallel}/V)$, the parameter needed to make the transformation, we have assumed[44]

$$\eta_{\parallel} = (F-B)/(F+B) \tag{2}$$

This assumes $v_{\perp} = 0$, and the fragment angular distribution in the moving frame is isotropic. We used standard formulas[45] to make the laboratory frame transformations for $d\sigma/d\Omega$ and $\theta$.

The values of $\eta_{\parallel}$ obtained from this procedure are shown in Figure 11. For the interaction of 44 MeV/nucleon $^{40}Ar$ with $^{197}Au$, we can compare these values with those measured directly by Pollacco, et al.[29] For the fission fragments (A=74-100), we deduce an average value of $\eta_{\parallel}$ of 0.42 $\pm$ 0.09. Pollaco et al. measure an average value of $\eta_{\parallel}$ of 0.38 with a most probable value (corresponding to a peripheral collision) of 0.21. While our work represents the first investigation of the 16 MeV/nucleon $^{32}S$ + $^{197}Au$ reaction, Patin et al.[13] did study the reaction of 19.6 MeV/nucleon $^{40}Ar$ with $^{197}Au$, finding two peaks in the fission folding angle distribution. These peaks corresponded to a central

collision peak at $\theta_{ff}$ = 107° (corresponding to $\eta_l$ = 0.69) and a peripheral collision peak at $\theta_{ff}$ = 151° (corresponding to $\eta_l$ = 0.32). These observations of the values of $\eta_l$ are in good agreement with our data for the 16 MeV/nucleon $^{32}S$ + $^{197}Au$ reaction. Bizard et al.[24] studied the 35 MeV/nucleon $^{40}Ar$ + $^{197}Au$ reaction and found two peaks in the folding angle distribution corresponding to $\eta_l$ = 0.82 and $\eta_l$ = 0.35, in fair agreement with our data.

The two peaks in the fission fragment folding angle distribution are reflected in the two-valued nature of $\eta_l$ (as a function of fragment mass). The high mass number portion of the fission mass yield distribution for the two lowest projectile energies studied in this work have $\eta_l$ values characteristic of central collisions while the low mass number portion of this distribution have $\eta_l$ values characteristic of peripheral collisions. For the highest projectile energy, fission (if defined as fragments in the central bump in the mass yield curve) occurs only with $\eta_l$ characteristic of peripheral collisions.

The heavy residues have $\eta_l$ values that are high ($\eta_l > 0.8$). It is important to remember that $\eta_l$ is that ratio of the velocity of the moving frame, $v_l$, to that of the fragment in the moving frame, V. Thus, the values of $\eta_l$ for heavy residues which have low velocities in the lab and moving frame[40] and the fission fragments which have high velocities may imply quite different momentum transfers in the primary projectile-target interaction.

The angular distributions resulting from the moving frame distributions using $\eta_l$ as defined in equation (2) are shown in Figures 12, 13, and 14. Some of the moving frame distributions are not symmetric with respect to 90°. To determine the origin of this lack of symmetry, we adopted a different approach to the moving frame

distributions. As suggested by Poskanzer et al.,[46] we assumed

$$G^{-1}(\eta_{|}, \eta_{\perp}, \theta_L) = G_o^{-1}(\eta_{|}, \theta_L) - (1/4)\eta_{\perp}^2(3\cos^2\theta_L-1) \quad (3)$$

and

$$\cos\theta = \cos\theta_o - (1/2)\eta_{\perp}^2(1-(1/2)\cos\theta_L \sin^2\theta_L) \quad (4)$$

where G is the correct function for transforming from the lab to the moving frame system, $G_o(\eta_{|}, \theta_L)$ is the standard transformation function[45] for $\eta_{\perp}$ equal to zero. For all distributions that were not symmetric in the moving frame (Figs. 12-14), we searched over all values of $\eta_{|}$, and $\eta_{\perp}$ seeking to minimize $(F/B)_{MF}$. We did not find any combination of $\eta_{|}$ and $\eta_{\perp}$ that symmetrized the asymmetric moving frame distributions. We conclude that the intermediate mass fragments (such as $^{46}$Sc and $^{48}$V in the $^{40}$Ar induced reactions) have moving frame distributions that are not symmetric with respect to a plane normal to the beam direction. This characteristic has been observed before[32,33] in reactions induced by 86 MeV/nucleon $^{12}$C. It means that the dominant mechanism giving rise to these fragments is "fast", i.e., the intermediate species does not live long enough that the statistical assumption is valid, i.e., a statistically large number of overlapping levels with randomly distributed phases is populated so interferences between them cancel. It has been estimated[47] that "fast" means < 2-3 x $10^{-23}$ sec.

The low mass number nuclides in the fission distributions in the two lowest energy reactions and all members of the fission distribution in the highest energy reaction have moving frame distributions that are, on average, symmetric in the moving frame. Presumably this is due to the slow nature of the normal fission process. The

highest mass number nuclides in the fission distribution at the lower projectile energies (which have large $\eta_l$ values corresponding to central collisions) have angular distributions that are asymmetric in the moving frame indicating the occurrence of a "fast" nuclear reaction. The observation about this lack of symmetry for the high A nuclides may seem puzzling at first glance. Since "normal" slow fission will produce these nuclides, why don't they have symmetric distributions? It may be argued[37] there are two processes contributing to the production of these high A nuclides, a normal slow fission process and a fast, non-equilibrium process. The fraction of events due to the fast, non-equilibrium process masks or distorts the symmetric angular distribution of the "normal" fission events.

At all energies the heavy residues result from fast, non-equilibrium processes. There is no kinematic complementarity between the intermediate mass fragments and the heavy residues as seen[33] as in the interaction of 86 MeV/nucleon $^{12}C$ with $^{238}U$. This observation indicates the production of intermediate mass fragments in a binary process in these reactions is not so probable as to be seen in the gross heavy residue distributions.

## IV. Discussion

The most unexpected aspect of the data presented in Section III is the observation of a fast, non-equilibrium production mechanism for the heavy fission fragments. One possible mechanism with these characteristics is that of "fast fission"[28]. In this mechanism, partial waves that exceed the rotating liquid drop limit at which point

the fission barrier vanishes ($\ell_{Bf=0}$) but that are less than the critical angular momentum ($\ell_{crit}$)) would lead to "fast fission". The characteristics of such a mechanism would be the large momentum transfer (due to $\ell < \ell_{crit}$) and a large mass asymmetry due to the fact the fusing nuclei never form a compound nucleus but re-separate on a fast time scale. For the reactions of 16 MeV/nucleon $^{32}S$ and 32 MeV/nucleon $^{40}Ar$ with $^{197}Au$, the values of $\ell_{Bf=0}$,$\ell_{crit}$, and $\ell_{max}$ are 66,96,256; and 65,113,499, respectively,[39] assuring the conditions for fast fission are met. (The values of $Z_{proj}Z_{tgt}$ are 1264 and 1422). Detailed calculations[6] confirm the possibility of fast fission for similar reactions such as the reaction of 27 MeV/nucleon $^{28}Si$ and $^{40}Ar$ with $^{238}U$. The occurrence of fast fission could be the cause of the unusually broad fission mass distribution for the reaction of 16 MeV/nucleon $^{32}S$ with $^{197}Au$ as well as the high $\eta_l$ values observed for the most asymmetric mass splits. Such a mechanism would lead naturally to the lack of symmetry in the moving frame distributions. However, there is one serious objection to this proposed mechanism. The strongly forward-peaked nature of the "fast" component angular distributions is contrary to that associated with "fast" fission.[28]

## V. Summary

We have measured the target fragment production cross sections and angular distributions for the reaction of 16 MeV/nucleon $^{32}S$, 32 MeV/nucleon and 44 MeV/nucleon $^{40}Ar$ with $^{197}Au$. From the measured fragment yields, we deduced the fragment isobaric yield distributions.

We observed large yields of the heavy residues from these collisions, indicating that counter experiments performed to data may have missed a significant fraction of all

such events due to a velocity cutoff. Due to the lack of symmetry about 90° in the moving frame angular distributions, we conclude that these fragments are produced in fast, non-equilibrium processes.

We have further observed that the ratio of yields of heavy residues to the yields of fission fragments increases with increasing projectile energy. The portion of the fission mass distribution due to high momentum transfer, central collisions involves a fast non-equilibrium process. The portion of the fission mass distribution due to peripheral, low momentum transfer collisions involves a slow process in which statistical equilibrium is established. The portion of the fission distribution due to central collisions is present at 16 and 32 MeV/nucleon but not at 44 MeV/nucleon.

Production of the intermediate mass fragments is a fast process without the establishment of statistical equilibrium at projectile energies of 32 and 44 MeV/nucleon.

Acknowledgements

We wish to thank J.F. Kepinski and G. Le Scornet for their technical assistance during the experiments at GANIL. At MSU, we gratefully acknowledge the help of Dr. R. Ronningen in helping us measure the short-lived activities. At LBL, we are grateful for the assistance of Ms. Ruth Mary Larimer. At all the accelerators, we appreciate the efforts of the operations and health physics personnel who made these measurements possible. Mr. Ru Shan Wang and Mr. Magnus Bergstrom aided in the data analysis at Oregon State. This work was supported in part by the U.S. Department of Energy under Contract Nos. DE-AMO6-76RLO2227, Task Agreement No.

DE-ATO6-76ER70035 and DE-ACO3-76SF00098, and the Swedish Natural Sciences Research Council.

References


1. S. Levit in Proc. Int'l Nucl. Phys. Conf. Harrogate, J.L. Durell, J.M. Irvine, and G.C. Morrison, ed. (Institute of Physics, Bristol, 1987) p. 227.
2. M. Conjeaud, S. Harar, M. Mostefai, E.C. Pollaco, C. Volant, Y. Cassagnou, R. Dayras, R. Legrain, H. Oeschler, and F. Saint-Laurent, Phys. Lett. 159B, 244 (1985).
3. S. Harar, Nucl. Phys. A471, 205c (1987).
4. B. Tamain, in Proc. Int'l Nucl. Phys. Conf., Harrogate, J.L. Durell, J.M. Irvine, and G.C. Morrison, ed. (Institute of Physics, Bristol, 1987) p. 247.
5. F. Hubert, R. Del Moral, J.P. Dufour, H. Emmermann, A. Fleury, C. Poinot, M.S. Pravikoff, H. Delagrange, and A. Lleres, Nucl. Phys. A456, 535 (1986).
6. H. Delagrange, C. Gregoire, Y. Abe, and N. Carjan, J de Physique, 47, C4-305 (1986).
7. J. Blachot, J. Crancon, B. deGoncourt, A. Gizon, and A. Lleres, Z. Phys. A321, 645 (1985).
8. H. Nifenecker, J. Blachot, J. Crancon, A. Gizon, and A. Lleres, Nucl. Phys. A447, 533c (1985).
9. D. Jacquet, et al., Phys. Rev. Lett. 53, 2226 (1984).
10. W.P. Zank, D. Hilscher, G. Ingold, U. Jahnke, M. Lehmann, and H. Rossner, Phys. Rev. C33, 519 (1986).
11. D. Guerreau, Nucl. Phys. A447, 37c (1985).
12. C. Cerruti, et al., Nucl. Phys. A453, 175 (1986).
13. Y. Patin, et al., Nucl. Phys. A457, 146 (1986).

14. K. Kwiatkowski, Nucl. Phys. A471, 271c (1987).

15. See, for example, J. Pochodzalla, Nucl. Phys. A471, 289c (1987); W.G. Lynch, ibid, 309c; D. Gross and H. Massman, ibid, 339c; J. P. Bondorf, et al., Nucl. Phys. A444, 460 (1985).

16. C. Gregoire, D. Jacquet, M. Pi, B. Remaud, F. Sebille, E. Suraud, P. Schuck, and L. Vinet, Nucl. Phys. A471, 399c (1987).

17. V.E. Viola, ibid, 53c.

18. H. Delagrange and J. Peter, ibid, 111c.

19. D. Fabris, et al., ibid, 351c.

20. G. Auger, et al., Phys. Lett. 169B, 161 (1986).

21. S. Leray, J. de Physique, 47, C4-273 (1986).

22. A. Lleres, C. Guet, D. Heuer, M. Maurel, C. Ristori, F. Schussler, M.W. Curtain and D.K. Scott, Phys. Lett. B185, 336 (1987).

23. G. Bizard, et al., Z. Phys. A323, 459 (1986).

24. G. Bizard, et al., Nucl. Phys. A456, 173 (1986).

25. B. Borderie, et al., Nouvelles du GANIL, No. 22 (1987).

26. D.J. Fields, et al., Phys. Rev. C34, 536 (1986).

27. M.F. Rivet, B. Borderie, H. Gauvin, D. Gardes, C. Cabot, F. Hannappe and J. Peter, Phys. Rev. C34, 1282 (1986).

28. C. Gregoire, C. Ngo, and B. Remaud, Nucl. Phys. A383, 392 (1982).

29. E.C. Pollacco, M. Conjeaud, S. Harar, C. Volant, Y. Cassagnou, R. Dayras, R. Legrain, M.S. Nguyen, H. Oeschler, and F. Saint-Laurent, Phys. Lett 146B, 29 (1984).

30. J. Blachot, et al. as cited in Ref. 21.

31. R. Wada, et al., Phys. Rev. C39, 497 (1989).

32. R. H. Kraus, Jr., W. Loveland, K. Aleklett, P.L. McGaughey, T.T. Sugihara, G.T. Seaborg, T. Lund, Y. Morita, E. Hagebo, and I.R. Haldorsen, Nucl. Phys. A432, 525 (1985).

33. K. Aleklett, W. Loveland, T. Lund, P.L. McGaughey, Y. Morita, G.T. Seaborg, E. Hagebo, and I. Haldorsen, Phys. Rev. C33, 885 (1986).

34. D.J. Morrissey, D. Lee, R.J. Otto, and G.T. Seaborg, Nucl. Instr. Meth. 158, 499 (1978).

35. D.J. Morrissey, W. Loveland, M. de Saint-Simon and G.T. Seaborg, Phys. Rev. C21, 1783 (1980).

36. K. Aleklett, W. Loveland, T.T. Sugihara, A.N. Behkami, D.J. Morrissey, Li Wenxin, Wing Kot, and G.T. Seaborg, Phys. Scr. 34, 489 (1986).

37. W. Loveland, K. Aleklett, L. Sihver, Z. Xu, C. Casey, and G.T. Seaborg, Nucl. Phys. A471, 175c (1987).

38. W. Loveland, K. Aleklett, P.L. McGaughey, K.J. Moody, R.M. McFarland, R.H. Kraus, Jr., and G.T. Seaborg, Lawrence Berkeley Laboratory Report LBL-16280, July, 1983.

39. W.W. Wilcke, J.R. Birkelund, H.J. Wollersheim, A.D. Hoover, J.R. Huizenga, W.U. Schroder, and L.E. Tubbs, At. Data and Nucl. Data Tables 25, 391 (1980).

40. K. Aleklett, M. Johannson, L. Sihver, W. Loveland, H. Groening, P.L. McGaughey, and G.T. Seaborg, Nuc. Phys. A489, 591 (1989).

41. C. Ceruti, R. Boisgard, C. Ngô and J. Desbois, Nucl. Phys. A492, 322 (1989).

42. K. Aleklett, W. Loveland, C. Casey, J.O. Liljenzin, D.J. Morrissey, M. de Saint-Simon, G.T. Seaborg, and L. Sihver, Nucl. Phys. (in preparation).

43. A. Van Den Berg, K.E. Rehm, D.G. Kovar, W. Kutschera, and G.S.F. Stephans, Phys. Lett. B194, 334 (1987).

44. J. M. Alexander in Nuclear Chemistry, Vol. I, L. Yaffe, ed. (Academic, New York, 1968) p.273.

45. J.B. Marion, T.I. Arnette, and H.C. Owens, Oak Ridge National Laboratory Report ORNL-2574, 1959.

46. A.M. Poskanzer, J.B. Cumming, and R. Wolfgang, Phys. Rev. 129, 374 (1963).

47. G.D. Harp, J.M. Miller, and B.J. Berne, Phys. Rev. 165, 1166 (1968).

48. C. Ngô, J. Peter, B. Tamain, M. Berlanger, and F. Hanappe, Z. Phys. A283, 161 (1976).

49. E. Duek, M. Rajagopalan, J.M. Alexander, T.W. Debiak, L. Kowalski, D. Logan, M. Kaplan, M. Zisman, and Y. Le Beyec, Z. Phys. A307, 237 (1982).

50. Z. Zheng, B. Borderie, D. Gardes, H. Gauvin, F. Hanappe, J. Peter, M.F. Rivet, B. Tamain, and A. Zaric, Nucl. Phys. A422, 447 (1984).

TABLE I.
Irradiation Conditions

| Accelerator | Particle | Length of Irradiation (min) | Total Number of Particles | Target Thickness ($mg/cm^2$) |
|---|---|---|---|---|
| LBL 88" Cyclotron | 16 MeV/N $^{32}S$ | 60 (yields) | $7.72 \times 10^{13}$ | 25.6 |
| | | 262 (yields) | $2.84 \times 10^{14}$ | 24.2 |
| | | 863(ang.dis.) | $5.41 \times 10^{15}$ | 0.150 |
| MSU K500 | 32 MeV/N $^{40}Ar$ | 192 (yields) | $5.69 \times 10^{13}$ | 48.5 |
| | | 1505(ang.dis.) | $4.48 \times 10^{14}$ | 0.270 |
| GANIL | 44 A MeV/N $^{40}Ar$ | 1057 | $5.69 \times 10^{15}$ | 0.300 |

TABLE II

Target fragment formation cross sections (mb) for the fragmentation of Au by 16 MeV/nucleon $^{32}S$, 32 MeV/nucleon and 44 MeV/nucleon $^{40}Ar$. Independent yields are indicated by (I); other yields are cumulative.

| Nuclide | Reaction: 16MeV/nucleon $^{32}S+^{197}Au$ (mb) | 32MeV/nucleon $^{40}Ar+^{197}Au$ (mb) | 44MeV/nucleon $^{40}Ar+^{197}Au$ (mb) |
|---|---|---|---|
| $^{38}S$(I) | 1.6 ± 0.1 | | |
| $^{42}K$ (I) | 6.1 ± 0.3 | 15.9 ± 0.4 | 16.4 ± 0.8 |
| $^{43}K$ | 13.6 ± 8.4 | 10.2 ± 0.2 | 13.5 ± 0.7 |
| $^{44}Sc$ | | | 1.8 ± 0.2 |
| $^{44}Sc^{m}$ (I) | | 4.9 ± 0.1 | 8.4 ± 1.2 |
| $^{46}Sc$ | 6.6 ± 0.4 | | 13.5 ± 1.3 |
| $^{47}Ca$ | 1.4 ± 0.1 | 6.5 ± 0.2 | |
| $^{47}Sc$ | | | 12.8 ± 0.7 |
| $^{48}Sc$ (I) | 3.2 ± 0.2 | 6.9 ± 0.2 | 3.8 ± 0.2 |
| $^{48}V$ | 1.4 ± 0.1 | 2.8 ± 0.2 | 4.5 ± 0.3 |
| $^{52}Mn$ | | 2.2 ± 0.1 | |
| $^{56}Mn$ | 7.8 ± 0.4 | | 10.0 ± 0.4 |
| $^{58}Co$ | 6.8 ± 0.4 | 12.2 ± 0.5 | 8.7 ± 0.2 |
| $^{59}Fe$ (I) | | 13.5 ± 0.6 | 7.2 ± 0.2 |
| $^{67}Ga$ | 4.2 ± 0.2 | 8.3 ± 0.4 | |
| $^{69}Ge$ | 5.8 ± 0.6 | | |
| $^{69}Zn^{m}$ (I) | | 10.2 ± 0.3 | |
| $^{71}As$ | 4.0 ± 0.4 | | 5.4 ± 0.4 |
| $^{72}Ga$ | 2.8 ± 0.1 | 11.6 ± 0.5 | |
| $^{72}As$ | 13.9 ± 1.3 | 14.5 ± 0.5 | |
| $^{73}Se$ | 2.4 ± 0.1 | | |
| $^{74}As$ (I) | 16.7 ± 0.8 | 21.8 ± 0.4 | 10.8 ± 0.2 |
| $^{75}Se$ | 13.7 ± 0.7 | 20.8 ± 0.6 | 11.4 ± 0.2 |
| $^{76}As$ (I) | 16.0 ± 0.2 | 21.9 ± 0.6 | |
| $^{76}Br$ | 2.7 ± 0.3 | 9.6 ± 1.1 | 9.4 ± 0.4 |
| $^{77}Br$ | 12.1 ± 1.6 | 15.4 ± 0.6 | 11.4 ± 2.4 |
| $^{82}Br$ | 7.8 ± 0.5 | 11.1 ± 0.6 | 6.1 ± 0.5 |
| $^{82}Sr$ | 2.9 ± 0.23 | | |
| $^{82}Rb^{m}$ (I) | | 16.4 ± 0.8 | |
| $^{83}Rb$ | | 50.0 ± 1.8 | 23.1 ± 0.5 |
| $^{83}Sr$ | | | 9.2 ± 0.5 |
| $^{84}Rb$ (I) | 27.9 ± 1.5 | 31.9 ± 0.7 | 14.1 ± 0.3 |
| $^{86}Rb$ (I) | 9.2 ± 0.7 | 33.0 ± 0.7 | |
| $^{86}Y$ | 13.1 ± 0.7 | 20.5 ± 0.8 | 7.9 ± 0.4 |
| $^{86}Zr$ | | | 5.6 ± 0.4 |
| $^{87}Y$ | | 40.0 ± 0.9 | 26.6 ± 0.5 |

| Nuclide | 16 MeV/nucleon 32S+197Au | 32 MeV/nucleon $^{40}Ar+^{197}Au$ | 44 MeV/nucleon $^{40}Ar+^{197}Au$ |
|---|---|---|---|
| $^{88}Zr$ | | 20.6 ± 0.8 | |
| $^{88}Y$ | 29.5 ± 1.6 | 45.5 ± 4.2 | 15.5 ± 5.8 |
| $^{89}Zr$ | 24.0 ± 0.9 | | 20.9 ± 0.2 |
| $^{90}Nb$ | 9.6 ± 0.5 | 18.2 ± 1.2 | 9.8 ± 0.4 |
| $^{93}Mo^{m}$ (I) | | 13.1 ± 1.2 | |
| $^{94}Tc$ | | 7.6 ± 1.1 | |
| $^{95}Tc$ | | 19.3 ± 0.4 | |
| $^{95}Zr$ | 7.9 ± 0.4 | | |
| $^{95}Nb$ | 19.7 ± 1.0 | | |
| $^{95}Nb^{m}$ | 1.3 ± 0.2 | | |
| $^{96}Tc$ | | 19.8 ± 0.7 | |
| $^{96}Nb$ (I) | 12.4 ± 0.5 | 13.3 ± 1.1 | |
| $^{97}Ru$ | | 14.6 ± 0.3 | 12.5 ± 0.3 |
| $^{99}Mo$ | 14.0 ± 0.5 | 11.4 ± 0.2 | 6.2 ± 0.2 |
| $^{100}Rh$ | 11.9 ± 0.6 | 14.3 ± 0.3 | 8.6 ± 0.5 |
| $^{100}Pd$ | | 8.2 ± 0.4 | |
| $^{101}Rh^{m}$ | | 19.6 ± 0.2 | |
| $^{103}Ru$ | 20.1 ± 1.3 | 14.1 ± 0.4 | 5.7 ± 0.3 |
| $^{105}Rh$ | 20.3 ± 1.1 | | 18.6 ± 0.4 |
| $^{105}Ag$ | 20.6 ± 2.6 | | 12.2 ± 0.3 |
| $^{106}Ag^{m}$ (I) | | 11.0 ± 1.1 | |
| $^{110}In$ | | 7.9 ± 0.6 | |
| $^{111}In$ | 23.7 ± 0.9 | 21.7 ± 1.0 | 15.2 ± 0.3 |
| $^{116}Te$ | 10.7 ± 0.5 | | 11.8 ± 0.6 |
| $^{117}Te$ | 14.3 ± 3.0 | | |
| $^{118}Sb^{m}$ (I) | | 5.6 ± 0.5 | |
| $^{119}Te$ | 9.4 ± 0.4 | | |
| $^{119}Te^{m}$ (I) | 10.0 ± 0.4 | | |
| $^{121}Te$ | 21.5 ± 1.8 | 19.1 ± 0.4 | 10.1 ± 0.5 |
| $^{121}Te^{m}$ (I) | 7.5 ± 2.0 | | |
| $^{122}Sb$ | 0.9 ± 0.1 | | |
| $^{122}Xe$ | 17.5 ± 2.6 | | |
| $^{123}I$ | | 18.6 ± 0.6 | |
| $^{123}Xe$ | 12.4 ± 0.6 | | |
| $^{125}Xe$ | | 12.4 ± 0.5 | |
| $^{126}Ba$ | | | 5.3 ± 0.8 |
| $^{127}Xe$ | 26.5 ± 1.5 | 22.0 ± 0.5 | |
| $^{128}Ba$ | 19.4 ± 0.9 | 18.1 ± 0.2 | 15.2 ± 0.7 |
| $^{131}Ba$ | 21.4 ± 1.8 | 18.9 ± 0.4 | 19.6 ± 0.4 |
| $^{132}La$ | 10.3 ± 0.5 | 31.6 ± 1.0 | 11.0 ± 0.6 |
| $^{132}Ce$ | 12.7 ± 0.6 | | 15.8 ± 0.9 |
| $^{135}Ce$ | 18.0 ± 1.1 | | 27.3 ± 1.1 |

| Nuclide | 16 MeV/nucleon 32S + 197Au | 32 MeV/nucleon $^{40}Ar + ^{197}Au$ | 44 MeV/nucleon $^{40}Ar + ^{197}Au$ |
|---|---|---|---|
| $^{139}Ce$ | 20.3 ± 1.0 | | |
| $^{143}Pr$ | | | 17.5 ± 2.4 |
| $^{145}Eu$ | 8.4 ± 0.4 | 17.9 ± 0.8 | 16.9 ± 0.4 |
| $^{146}Gd$ | 6.6 ± 0.9 | | 17.7 ± 0.4 |
| $^{147}Eu$ | 12.8 ± 2.3 | 16.5 ± 0.5 | 28.1 ± 1.2 |
| $^{147}Gd$ | 8.4 ± 0.6 | 16.0 ± 0.8 | 23.0 ± 1.0 |
| $^{149}Gd$ | 12.0 ± 1.1 | 14.5 ± 1.0 | 24.7 ± 0.5 |
| $^{151}Gd$ | | | 18.5 ± 0.9 |
| $^{151}Tb$ | 10.9 ± 2.3 | 15.9 ± 1.2 | 17.7 ± 0.8 |
| $^{152}Tb$ | 8.6 ± 0.4 | 13.0 ± 0.4 | |
| $^{152}Dy$ | | | 15.7 ± 1.1 |
| $^{153}Gd$ | | | 9.3 ± 0.6 |
| $^{153}Tb$ | 6.9 ± 0.8 | | 21.7 ± 0.6 |
| $^{155}Tb$ | 8.8 ± 0.5 | 12.7 ± 0.6 | 21.1 ± 0.6 |
| $^{155}Dy$ | 7.4 ± 0.4 | | 24.0 ± 1.2 |
| $^{157}Dy$ | 8.1 ± 0.4 | | 25.5 ± 1.2 |
| $^{158}Er$ | 8.6 ± 0.4 | | |
| $^{160}Er$ | 6.1 ± 0.9 | | 22.8 ± 1.1 |
| $^{165}Tm$ | | | 26.8 ± 6.8 |
| $^{167}Tm$ | 6.1 ± 0.3 | | 26.0 ± 0.6 |
| $^{169}Yb$ | 4.0 ± 0.2 | 19.8 ± 1.4 | 17.1 ± 0.4 |
| $^{169}Lu$ | 7.7 ± 0.5 | | |
| $^{170}Lu$ | 9.2 ± 1.1 | 26.7 ± 1.4 | |
| $^{170}Hf$ | | | 22.4 ± 1.0 |
| $^{171}Lu$ | 4.9 ± 0.3 | 17.9 ± 0.1 | 24.5 ± 0.5 |
| $^{171}Hf$ | 10.3 ± 2.7 | | |
| $^{173}Hf$ | 5.6 ± 0.2 | 16.9 ± 0.8 | |
| $^{174}Ta$ | 13.4 ± 0.7 | | |
| $^{175}Hf$ | | | 21.3 ± 0.5 |
| $^{175}Ta$ | | 26.2 ± 1.1 | |
| $^{176}Ta$ | | 33.0 ± 1.4 | |
| $^{181}Re$ | | 22.4 ± 0.6 | |
| $^{182}Re$ | 2.1 ± 0.3 | | |
| $^{182}Re^{m}$ (I) | 46.0 ± 14.2 | | |
| $^{182}Os$ | 3.4 ± 1.6 | | |
| $^{183}Re$ | | | 23.7 ± 0.6 |
| $^{183}Os^{m}$ | | 17.6 ± 0.7 | |
| $^{185}Os$ | | | 28.1 ± 0.7 |
| $^{185}Ir$ | | 42.4 ± 2.2 | 24.6 ± 2.0 |
| $^{186A}Ir$ | 12.4 ± 2.1 | 17.4 ± 0.6 | |
| $^{186B}Ir$ (I) | 13.9 ± 1.5 | | |
| $^{186}Pt$ | | | 14.5 ± 1.4 |

| Nuclide | 16 MeV/nucleon $^{32}S + ^{197}Au$ | 32 MeV/nucleon $^{40}Ar + ^{197}Au$ | 44 MeV/nucleon $^{40}Ar + ^{197}Au$ |
|---|---|---|---|
| $^{188}Pt$ | 10.8 ± 5.5 | | |
| $^{189}Ir$ | 21.5 ± 1.2 | | 31.9 ± 0.8 |
| $^{189}Pt$ | | 79.9 ± 7.1 | |
| $^{191}Pt$ | 45 ± 14 | 71.6 ± 1.9 | 42.1 ± 1.6 |
| $^{191}Au$ | 65 ± 3 | | 20.3 ± 1.8 |
| $^{192}Au$ | 55 ± 24 | | 24.0 ± 1.5 |
| $^{192}Hg$ | 31.0 ± 1.6 | | |
| $^{193}Hg$ | 10.7 ± 1.6 | | |
| $^{193}Hg^{m}$ | 18.2 ± 1.4 | 17.0 ± 0.7 | |
| $^{194}Au$ (I) | 26.8 ± 1.0 | 70.3 ± 3.3 | 46 ± 3 |
| $^{196}Au$ | 116 ± 12 | 177.7 ± 5.2 | 122 ± 3 |
| $^{196}Tl$ | 43.6 ± 2.3 | | |
| $^{196}Tl^{m}$ | 57 ± 11 | | |
| $^{198}Au$ | 20.8 ± 1.1 | | |
| $^{198}Au^{m}$(I) | 4.3 ± 0.3 | | |
| $^{199}Au$ | 14.1 ± 1.2 | | |

TABLE III
Charge Dispersion Parameters

| Fragment Mass Number Range | $Z_{mp}$ | $C_z$ |
|---|---|---|
| | 16 MeV/nucleon $^{32}S$ + $^{197}Au$ | |
| 38-58 | 0.440A + 0.499 | 0.6 |
| 67-77 | 0.439A + 0.516 | 0.6 |
| 82-90 | 0.433A + 0.923 | 0.8 |
| 95-105 | 0.420A + 1.95 | 1.0 |
| 111-122 | 0.416A + 2.46 | 0.8 |
| 123-139 | 0.376A + 7.36 | 1.0 |
| 145-155 | 0.385A + 6.96 | 1.0 |
| 160-174 | 0.400A + 3.30 | 0.4 |
| 182-191 | 0.375A + 6.96 | 0.3 |
| 192-199 | 0.375A + 5.40 | 0.6 |
| | 32 MeV/nucleon $^{40}Ar$ + $^{197}Au$ | |
| 42-44 | 0.443A + 0.584 | 0.5 |
| 47-59 | 0.435A + 0.924 | 0.7 |
| 67-77 | 0.428A + 1.37 | 0.7 |
| 82-90 | 0.422A + 1.82 | 1.0 |
| 93-106 | 0.412A + 2.80 | 1.2 |
| 110-121 | 0.404A + 3.63 | 0.5 |
| 123-132 | 0.393A + 5.19 | 0.7 |
| 145-149 | 0.341A + 13.5 | 1.0 |
| 151-155 | 0.333A + 14.5 | 0.5 |
| 169-176 | 0.317A + 17.3 | 0.3 |
| 181-189 | 0.294A + 22.3 | 0.3 |
| 191-196 | 0.311A + 18.7 | 0.7 |
| | 44 MeV/nucleon $^{40}Ar$ + $^{197}Au$ | |
| 42-44 | 0.443A + 0.661 | 0.7 |
| 46-59 | 0.435A + 0.924 | 0.5 |
| 71-77 | 0.428A + 1.37 | 0.7 |
| 82-90 | 0.422A + 1.82 | 1.0 |
| 97-105 | 0.412A + 2.80 | 1.0 |
| 111-121 | 0.404A + 3.63 | 1.0 |
| 126-143 | 0.402A + 4.03 | 0.7 |
| 145-149 | 0.382A + 7.02 | 1.0 |
| 151-160 | 0.357A + 10.72 | 0.7 |
| 165-175 | 0.317A + 17.3 | 0.6 |
| 183-189 | 0.294A + 22.3 | 0.9 |
| 191-196 | 0.311A + 18.7 | 0.7 |

Figure Captions

Figure 1. The independent yield distributions from the reaction of 16 MeV/nucleon $^{32}S$ with $^{197}Au$ (long irradiation). The plotted points are the independent yield cross sections calculated from the data while the solid lines are the Gaussian charge dispersions used in the calculation.

Figure 2. Same as Figure 1 except data are for the reaction of 32 MeV/nucleon $^{40}Ar$ with $^{197}Au$.

Figure 3. Same as Figure 1 except data are for the reaction of 44 MeV/nucleon $^{40}Ar$ with $^{197}Au$.

Figure 4. Isobaric yield distributions for the fragmentation of $^{197}Au$ by (a) 16 MeV/nucleon $^{32}S$ (b) 32 MeV/nucleon $^{40}Ar$ and (c) 44 MeV/nucleon $^{40}Ar$. (d) A comparison of the isobaric yield distributions from this work. The light ion data is from ref. 38.

Figure 5. Excitation functions for fission and heavy residue production for the $^{40}Ar$ + $^{197}Au$ reaction. The cross sections from the $^{32}S$ + $^{197}Au$ reaction have been scaled to the $^{40}Ar$ + $^{197}Au$ reaction by the ratio of the reaction cross sections.[39] Additional data from ref. 48, 49, and 50.

Figure 6. Laboratory frame angular distributions for near target residues for the reaction of $^{197}Au$ with (a) 32 MeV/nucleon $^{40}Ar$ (b) 44 MeV/nucleon $^{40}Ar$.

Figure 7. Laboratory frame angular distributions for representative fragments from the reaction of 16 MeV/nucleon $^{32}S$ with $^{197}Au$.

Figure 8. Same as Figure 7 except reaction is 32 MeV/nucleon $^{40}Ar$ with $^{197}Au$.

Figure 9. Same as Figure 7 except reaction is 44 MeV/nucleon $^{40}Ar$ with $^{197}Au$.

Figure 10. A comparison of the laboratory frame angular distributions for all the reactions studied.

Figure 11. Values of $\eta_l$ as a function of product mass number for all the reactions studied.

Figure 12. Moving frame angular distributions for the representative fragments from the interactions of 16 MeV/nucleon $^{32}S$ with $^{197}Au$.

Figure 13. Same as Figure 12 except the reaction is 32 MeV/nucleon $^{40}Ar$ with $^{197}Au$.

Figure 14. Same as Figure 12 except the reaction is 44 MeV/nucleon $^{40}Ar$ with $^{197}Au$.

Table Captions

Table I. Irradiation Conditions.

Table II. Target fragmentation formation cross sections (mb) for the fragmentation of Au by 16 MeV/N $^{32}S$, 32 MeV/N $^{40}Ar$ and 44 MeV/N $^{40}Ar$. Independent yields are indicated by (I); other yields are cumulative.

Table III. Charge Distribution Parameters.

KEYWORD ABSTRACT

NUCLEAR REACTIONS $^{197}(^{32}S, X)$, E = 512 MeV; $^{197}Au(^{40}Ar, X)$, E = 1280, 1760 MeV; measured $\sigma(Z, A, \theta)$; deduced $\sigma(A)$; intermediate energy heavy ions.

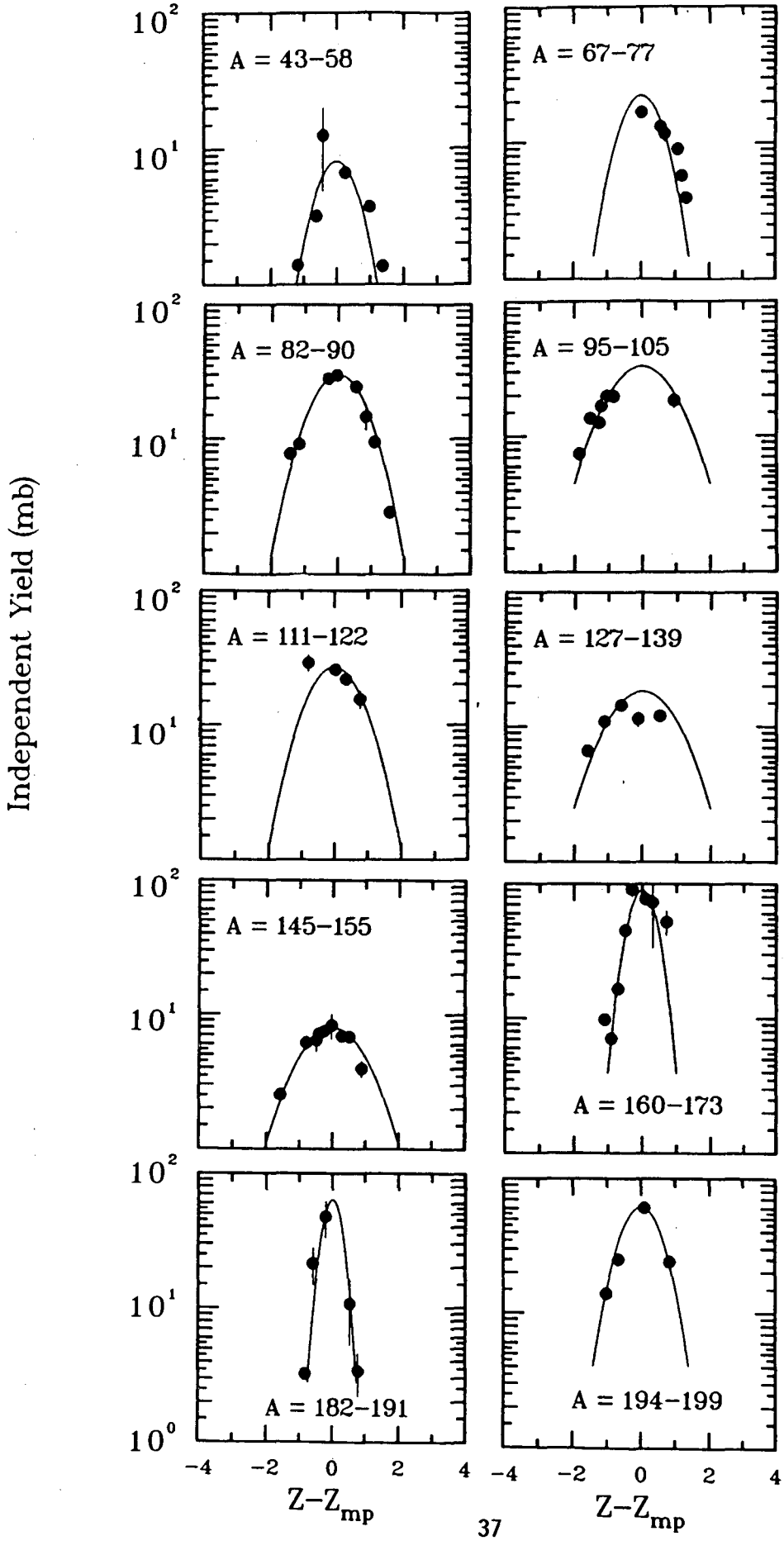
Independent Yield (mb)
A = 43–58
A = 67–77
A = 82–90
A = 95–105
A = 111–122
A = 127–139
A = 145–155
A = 160–173
A = 182–191
A = 194–199
$10^2$
$10^1$
$10^0$
−4
−2
0
2
4
$Z-Z_{mp}$

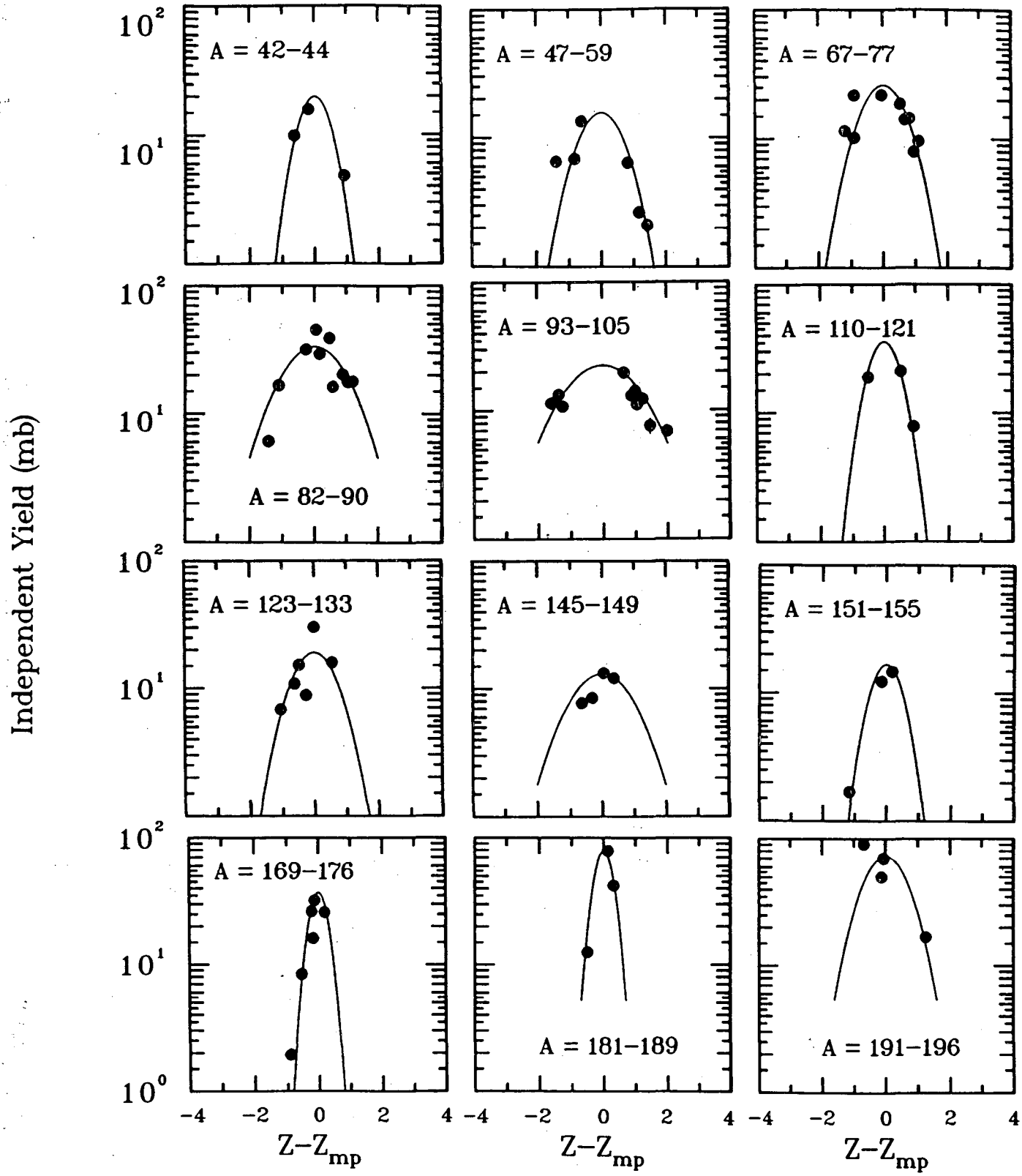
Independent Yield (mb)
A = 42–44
A = 47–59
A = 67–77
A = 82–90
A = 93–105
A = 110–121
A = 123–133
A = 145–149
A = 151–155
A = 169–176
A = 181–189
A = 191–196
$10^2$
$10^1$
$10^0$
−4 −2 0 2 4
$Z-Z_{mp}$

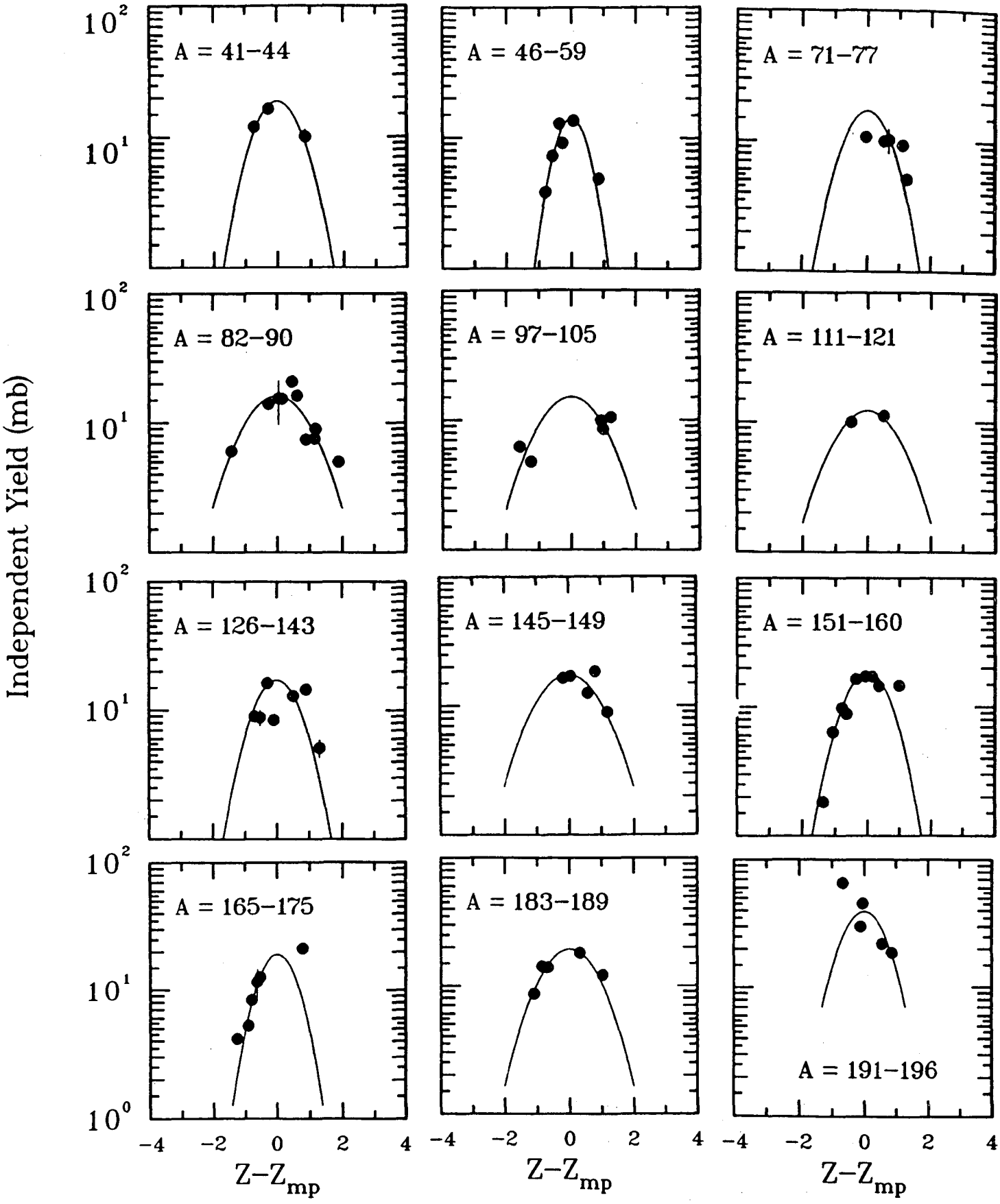
Independent Yield (mb)
A = 41–44
A = 46–59
A = 71–77
A = 82–90
A = 97–105
A = 111–121
A = 126–143
A = 145–149
A = 151–160
A = 165–175
A = 183–189
A = 191–196
$10^2$
$10^1$
$10^0$
−4
−2
0
2
4
$Z-Z_{mp}$

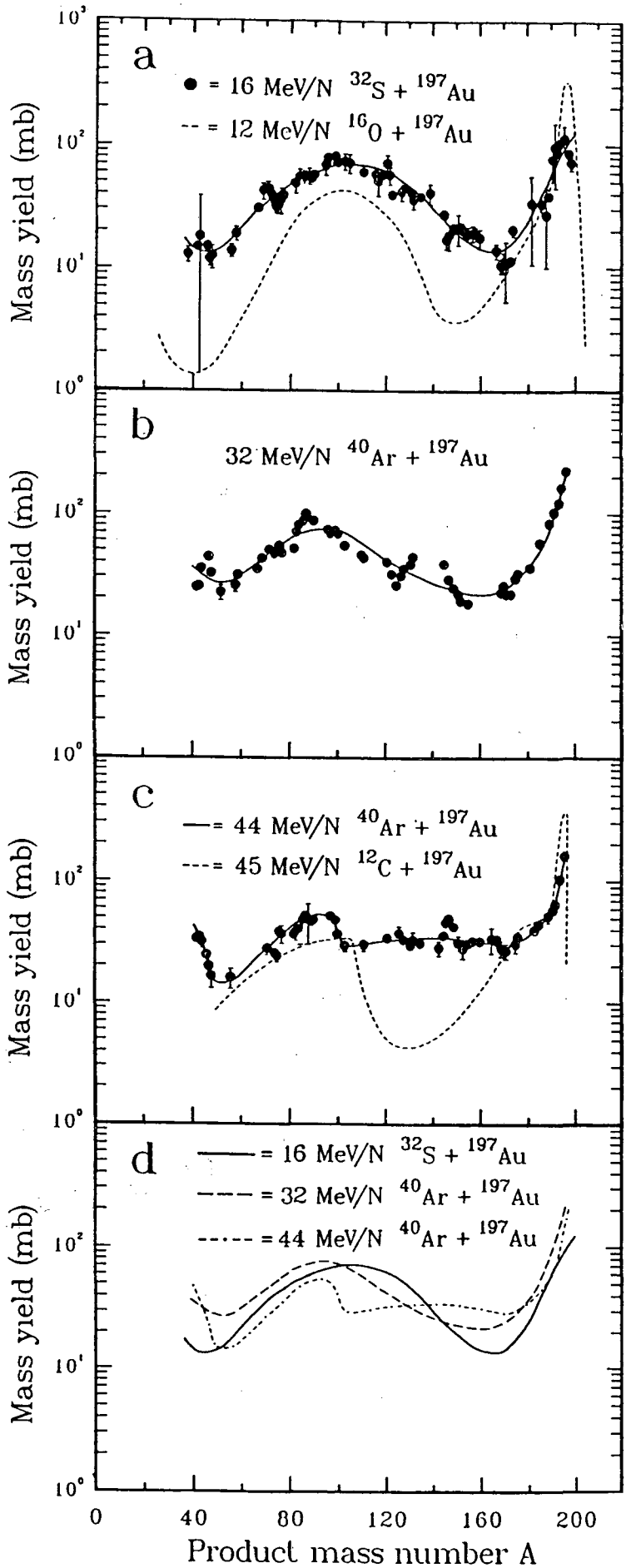
a
● = 16 MeV/N $^{32}S + ^{197}Au$
-- = 12 MeV/N $^{16}O + ^{197}Au$
b
32 MeV/N $^{40}Ar + ^{197}Au$
c
— = 44 MeV/N $^{40}Ar + ^{197}Au$
--- = 45 MeV/N $^{12}C + ^{197}Au$
d
— = 16 MeV/N $^{32}S + ^{197}Au$
— — = 32 MeV/N $^{40}Ar + ^{197}Au$
-·-·- = 44 MeV/N $^{40}Ar + ^{197}Au$
Mass yield (mb)
$10^3$
$10^2$
$10^1$
$10^0$
0
40
80
120
160
200
Product mass number A

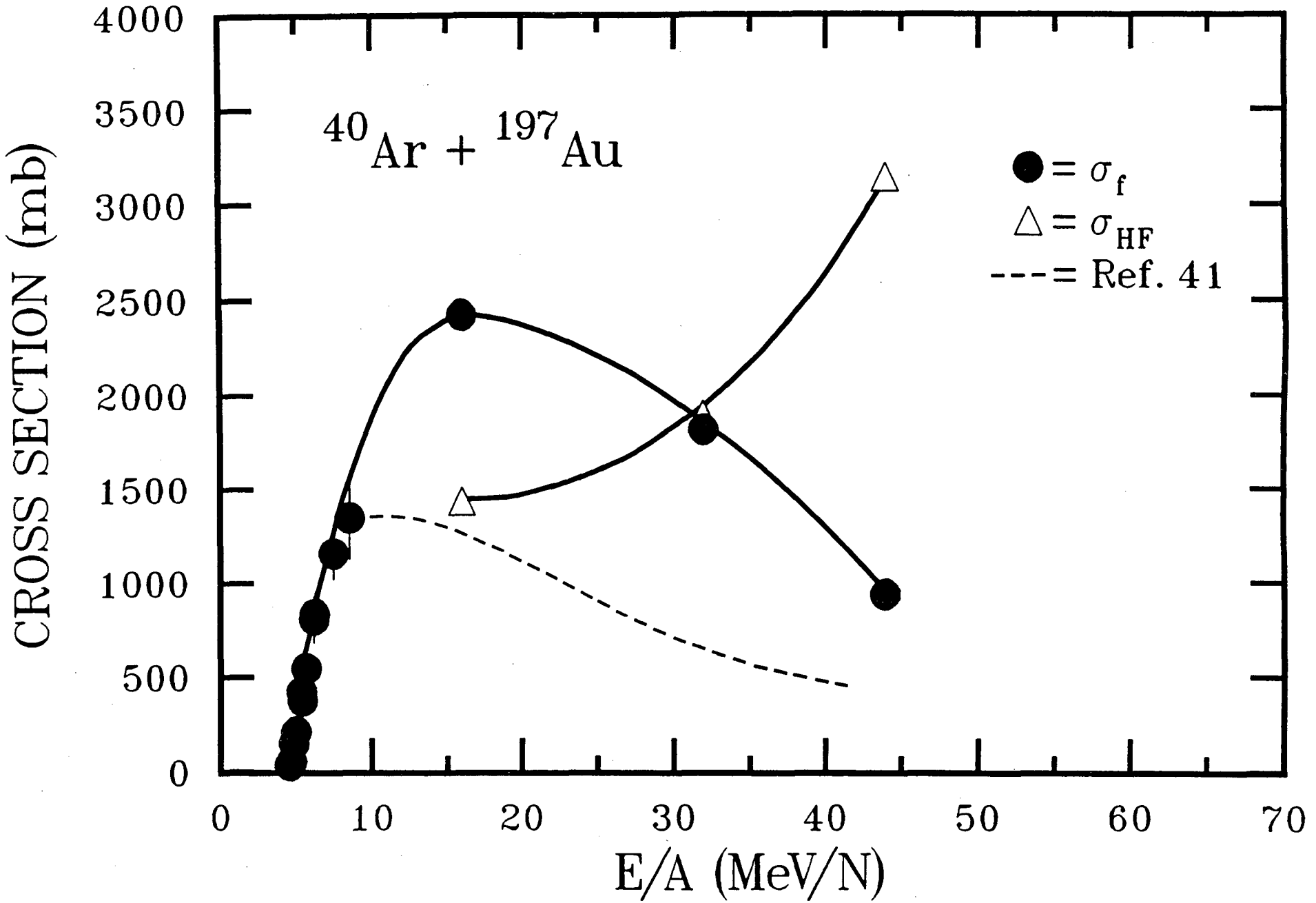
$^{40}Ar + ^{197}Au$
● = $\sigma_f$
△ = $\sigma_{HF}$
--- = Ref. 41
CROSS SECTION (mb)
E/A (MeV/N)
0
500
1000
1500
2000
2500
3000
3500
4000
0
10
20
30
40
50
60
70

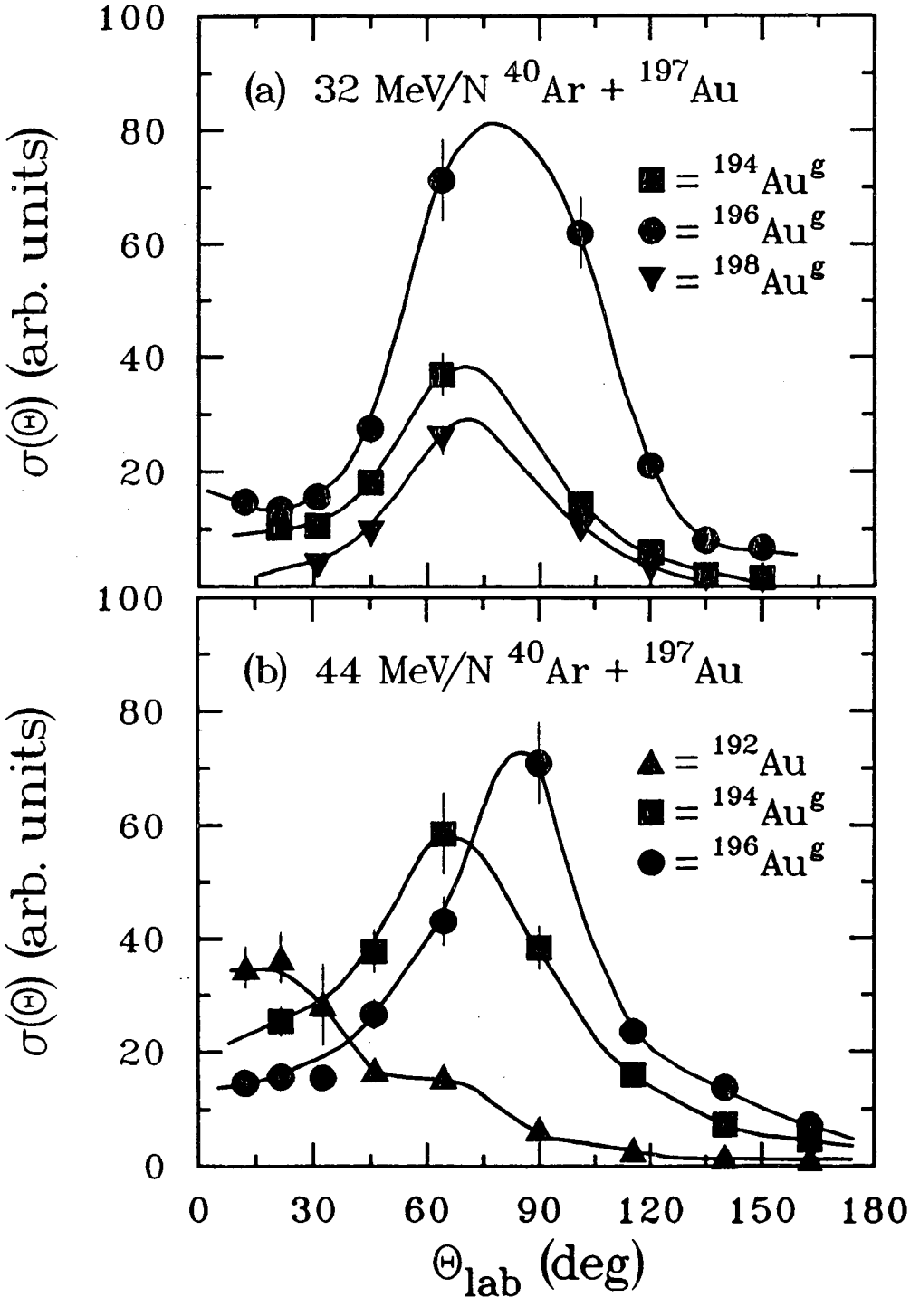
(a) 32 MeV/N $^{40}$Ar + $^{197}$Au
■ = $^{194}$Au$^{g}$
● = $^{196}$Au$^{g}$
▼ = $^{198}$Au$^{g}$
(b) 44 MeV/N $^{40}$Ar + $^{197}$Au
▲ = $^{192}$Au
■ = $^{194}$Au$^{g}$
● = $^{196}$Au$^{g}$
σ(Θ) (arb. units)
Θ$_{lab}$ (deg)
0
20
40
60
80
100
30
90
120
150
180

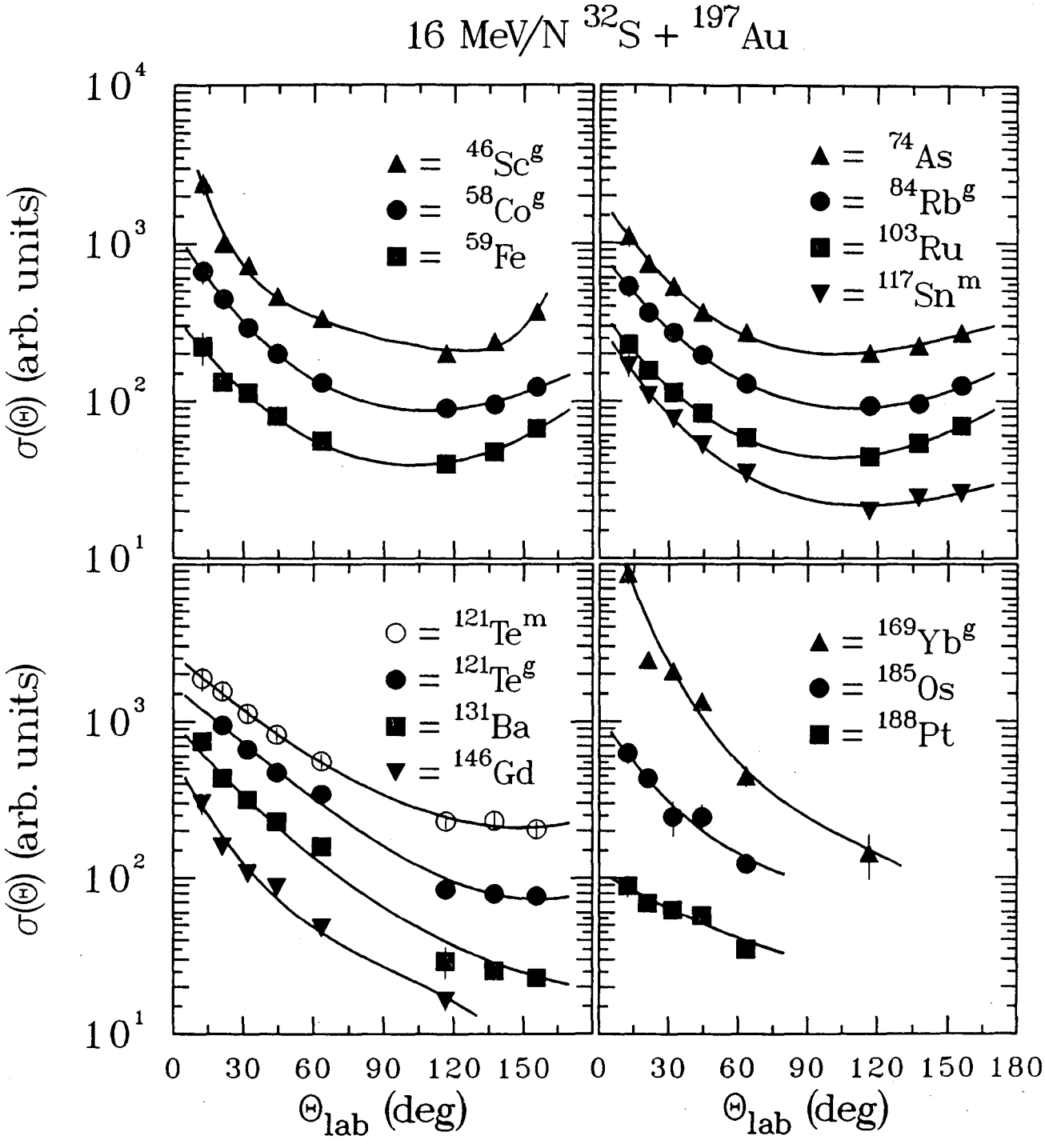
16 MeV/N $^{32}$S + $^{197}$Au
▲ = $^{46}$Sc$^{g}$
● = $^{58}$Co$^{g}$
■ = $^{59}$Fe
▲ = $^{74}$As
● = $^{84}$Rb$^{g}$
■ = $^{103}$Ru
▼ = $^{117}$Sn$^{m}$
○ = $^{121}$Te$^{m}$
● = $^{121}$Te$^{g}$
■ = $^{131}$Ba
▼ = $^{146}$Gd
▲ = $^{169}$Yb$^{g}$
● = $^{185}$Os
■ = $^{188}$Pt
σ(Θ) (arb. units)
$10^4$
$10^3$
$10^2$
$10^1$
0 30 60 90 120 150
0 30 60 90 120 150 180
$\Theta_{lab}$ (deg)

K. ALEKLETT
6-JUN-89

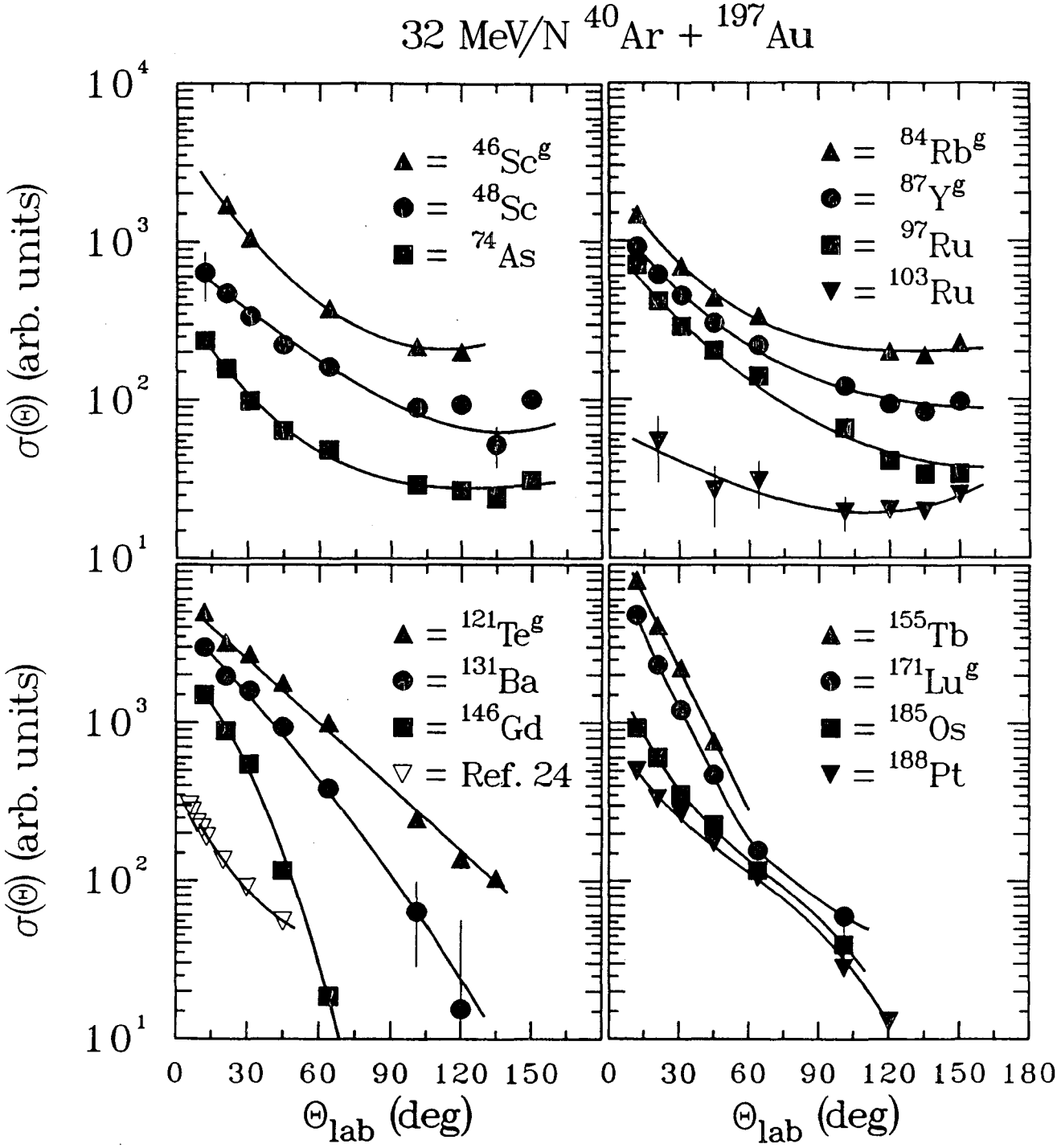

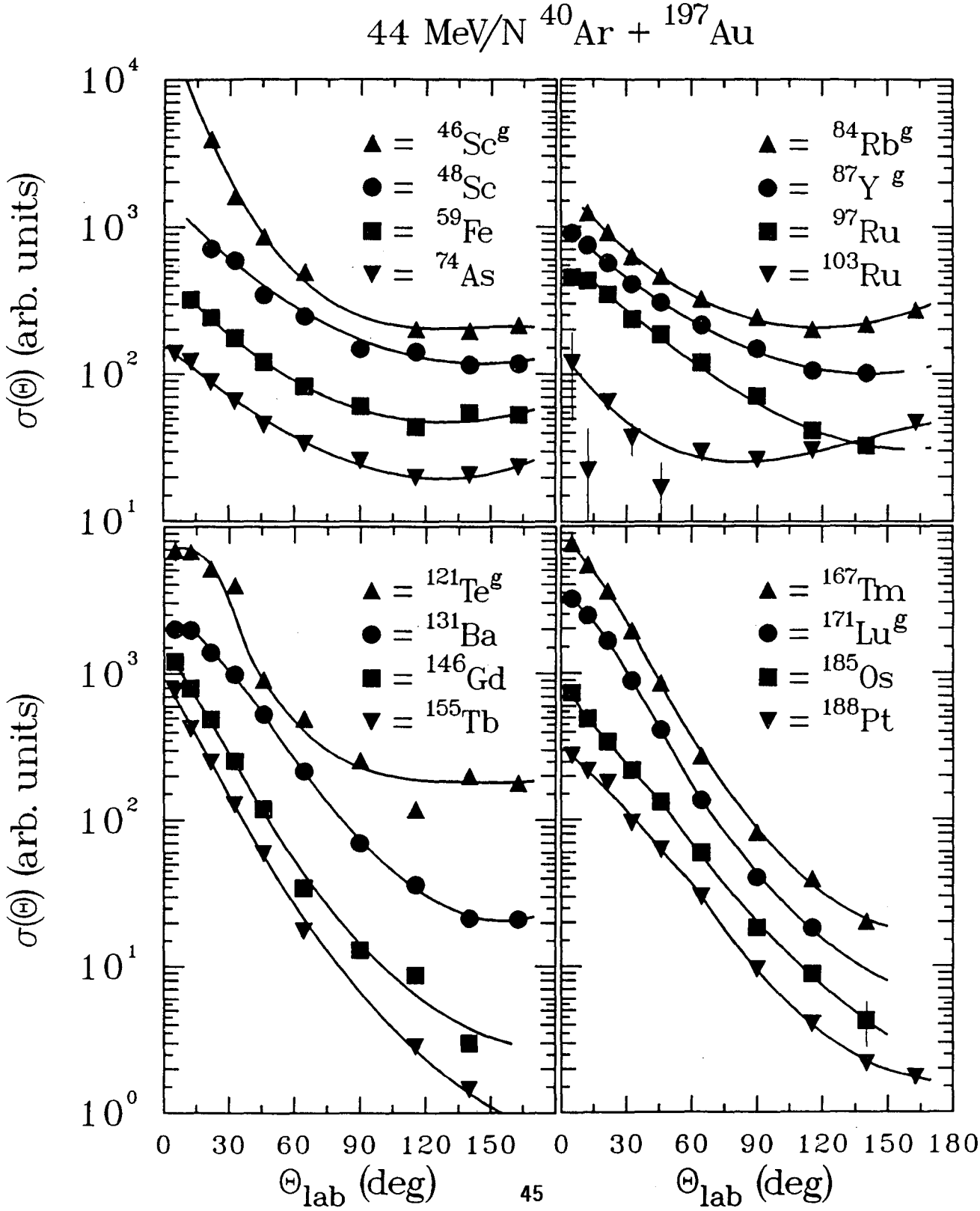
44 MeV/N $^{40}$Ar + $^{197}$Au
▲ = $^{46}$Sc$^{g}$
● = $^{48}$Sc
■ = $^{59}$Fe
▼ = $^{74}$As
▲ = $^{84}$Rb$^{g}$
● = $^{87}$Y$^{g}$
■ = $^{97}$Ru
▼ = $^{103}$Ru
▲ = $^{121}$Te$^{g}$
● = $^{131}$Ba
■ = $^{146}$Gd
▼ = $^{155}$Tb
▲ = $^{167}$Tm
● = $^{171}$Lu$^{g}$
■ = $^{185}$Os
▼ = $^{188}$Pt
$\sigma(\Theta)$ (arb. units)
$10^{4}$
$10^{3}$
$10^{2}$
$10^{1}$
$10^{0}$
0 30 60 90 120 150
0 30 60 90 120 150 180
$\Theta_{lab}$ (deg)

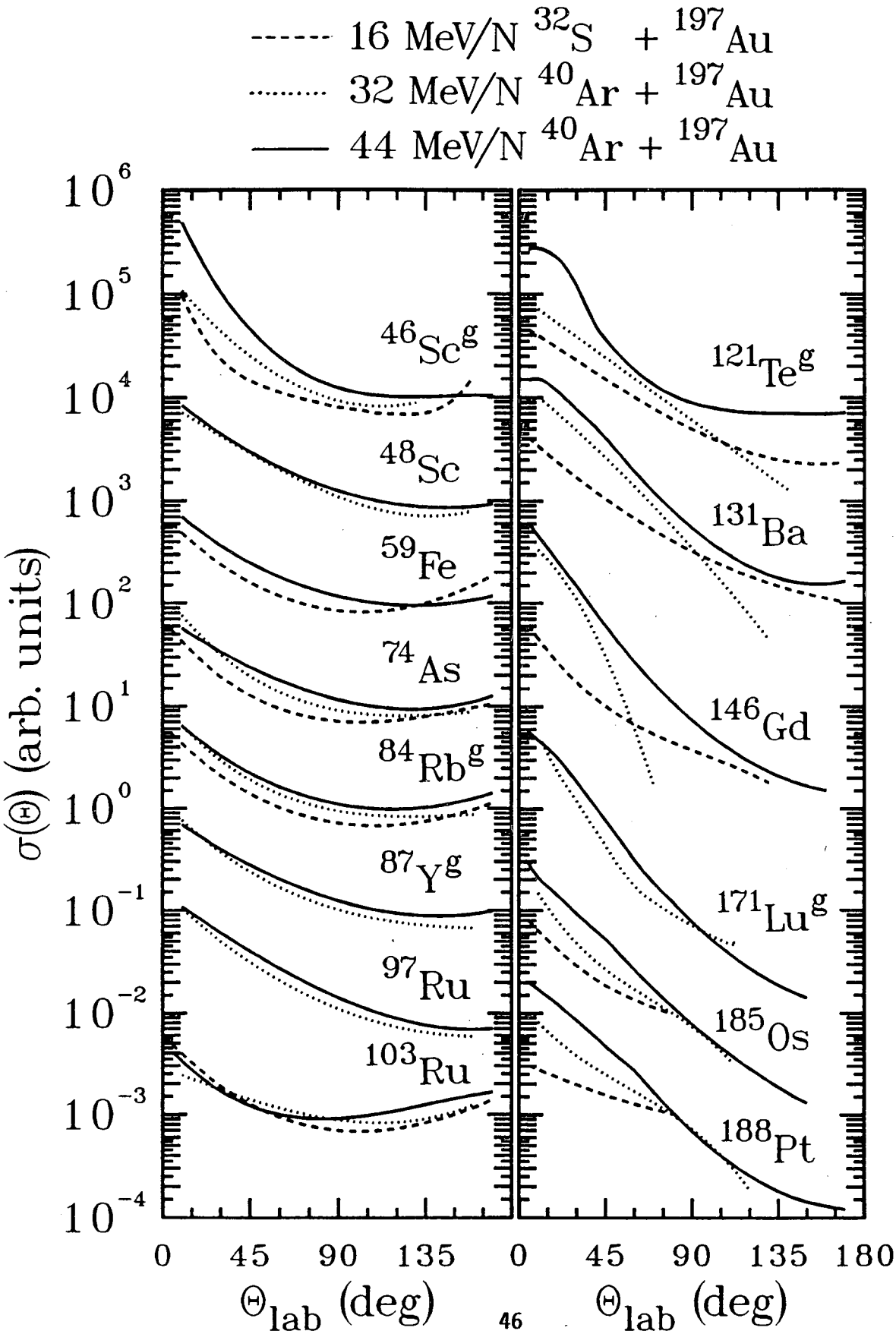
16 MeV/N $^{32}$S + $^{197}$Au
32 MeV/N $^{40}$Ar + $^{197}$Au
44 MeV/N $^{40}$Ar + $^{197}$Au
$\sigma(\Theta)$ (arb. units)
$10^{6}$
$10^{5}$
$10^{4}$
$10^{3}$
$10^{2}$
$10^{1}$
$10^{0}$
$10^{-1}$
$10^{-2}$
$10^{-3}$
$10^{-4}$
$^{46}$Sc$^{g}$
$^{48}$Sc
$^{59}$Fe
$^{74}$As
$^{84}$Rb$^{g}$
$^{87}$Y$^{g}$
$^{97}$Ru
$^{103}$Ru
$^{121}$Te$^{g}$
$^{131}$Ba
$^{146}$Gd
$^{171}$Lu$^{g}$
$^{185}$Os
$^{188}$Pt
0 45 90 135
0 45 90 135 180
$\Theta_{lab}$ (deg)
$\Theta_{lab}$ (deg)

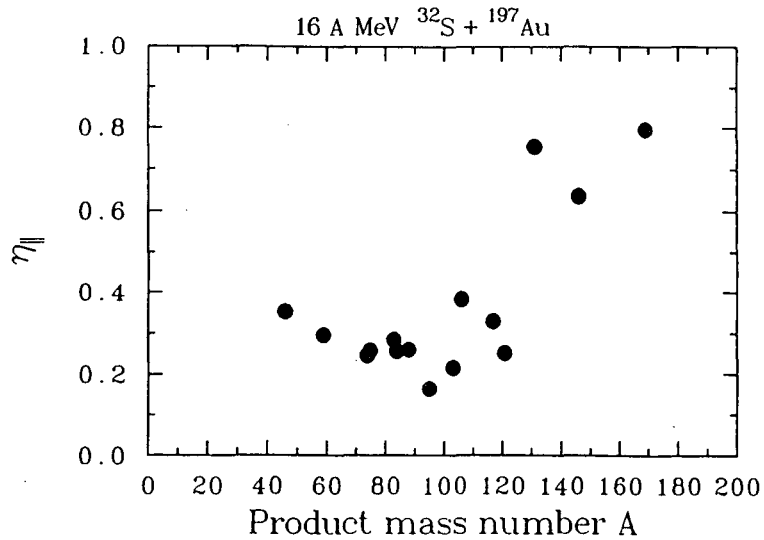
16 A MeV $^{32}S + ^{197}Au$
$\eta_{\parallel}$
1.0
0.8
0.6
0.4
0.2
0.0
0 20 40 60 80 100 120 140 160 180 200
Product mass number A

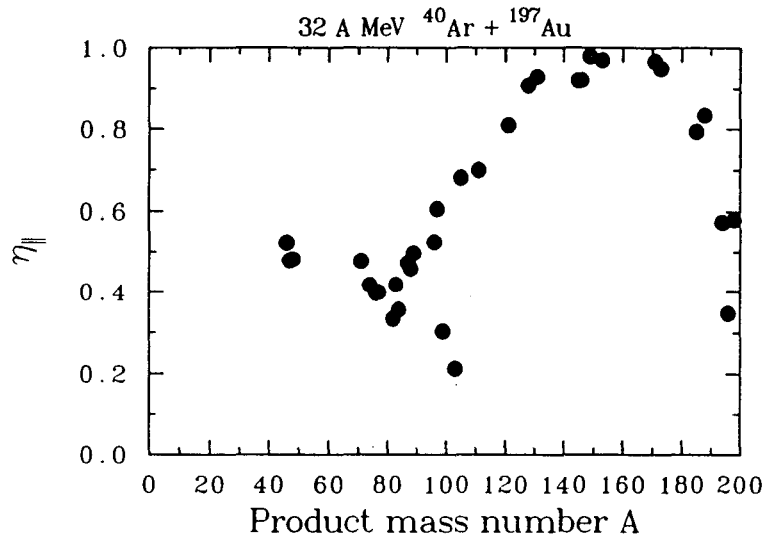
32 A MeV $^{40}Ar + ^{197}Au$
$\eta_{\parallel}$
1.0
0.8
0.6
0.4
0.2
0.0
0 20 40 60 80 100 120 140 160 180 200
Product mass number A

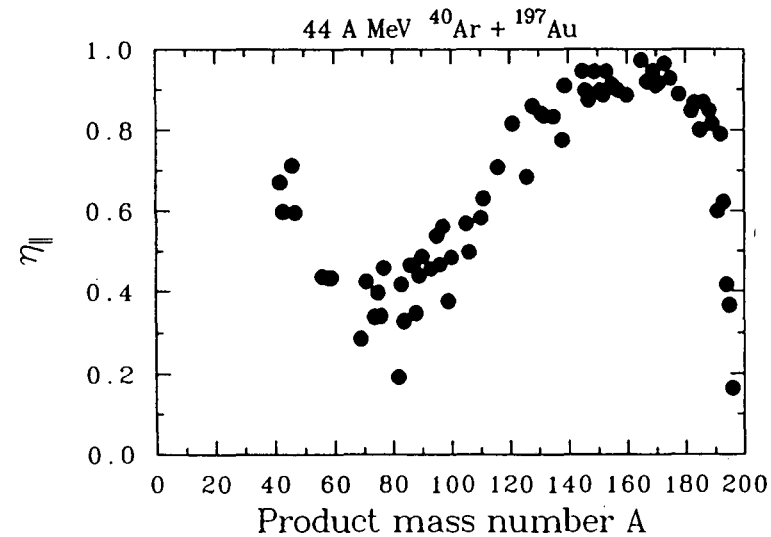
44 A MeV $^{40}Ar + ^{197}Au$
$\eta_{\parallel}$
1.0
0.8
0.6
0.4
0.2
0.0
0 20 40 60 80 100 120 140 160 180 200
Product mass number A

K. ALEKLETT
16-JUN-89

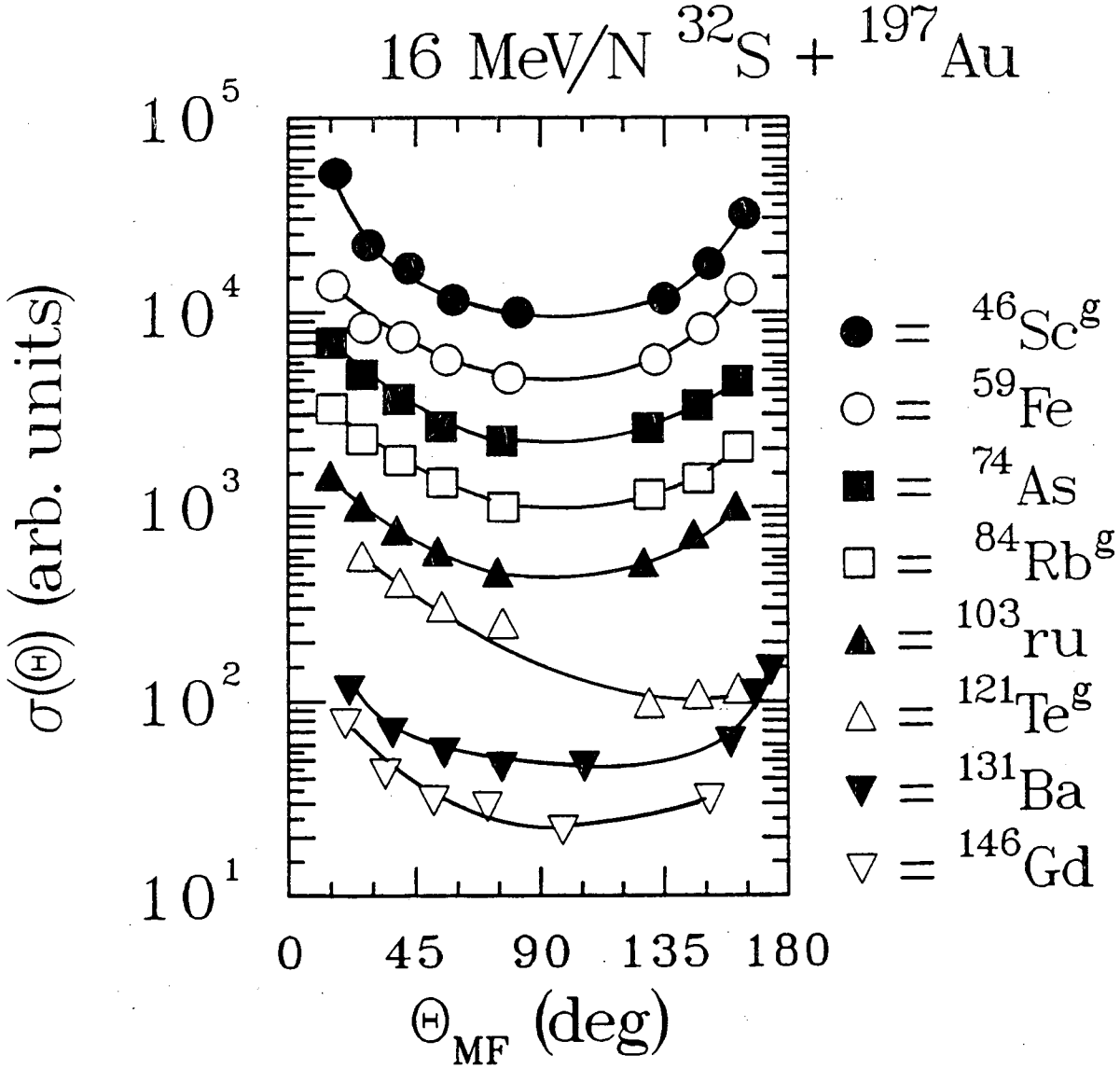

K. ALEKLETT
16-JUN-89

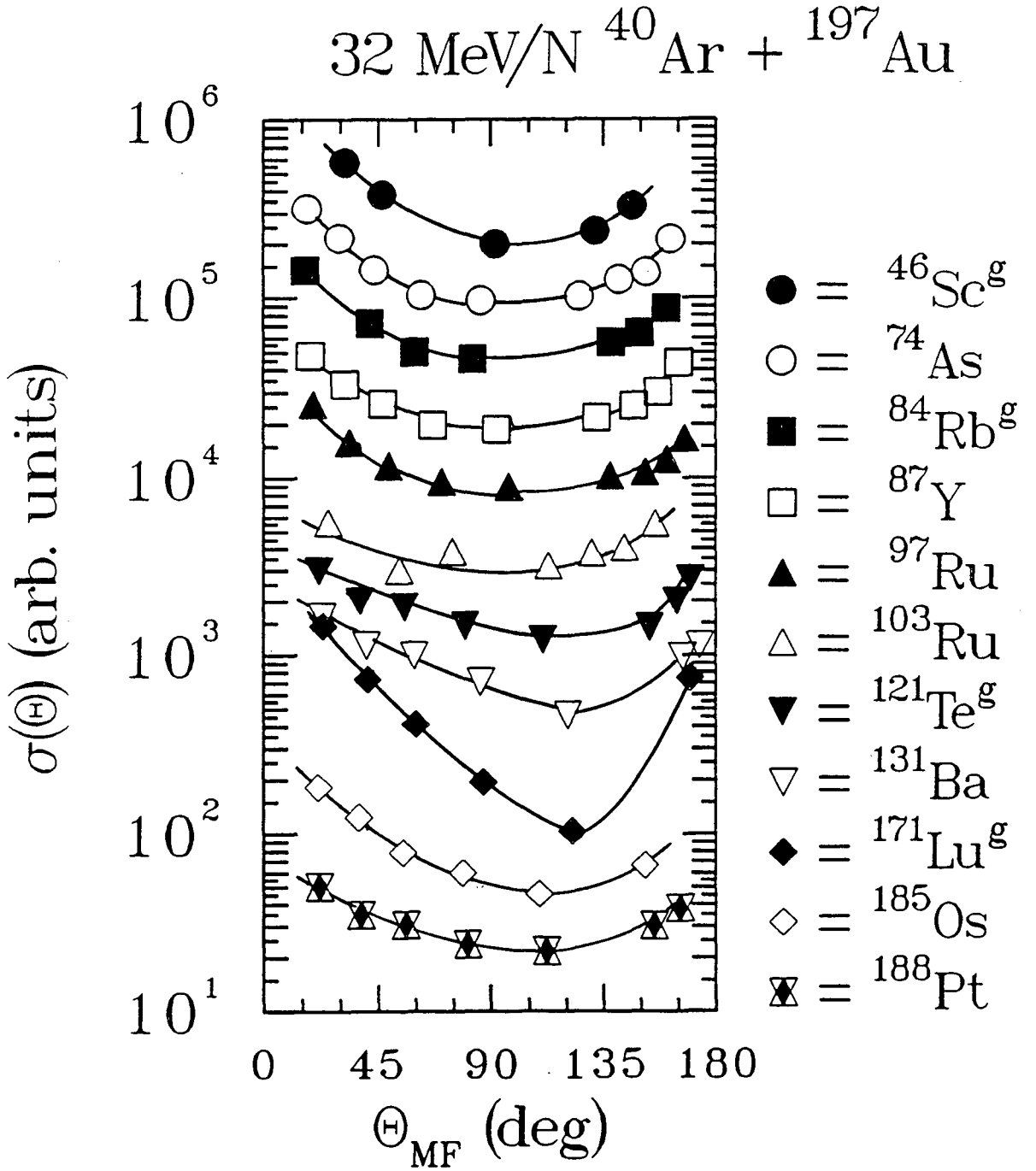

K. ALEKLETT
16-JUN-89

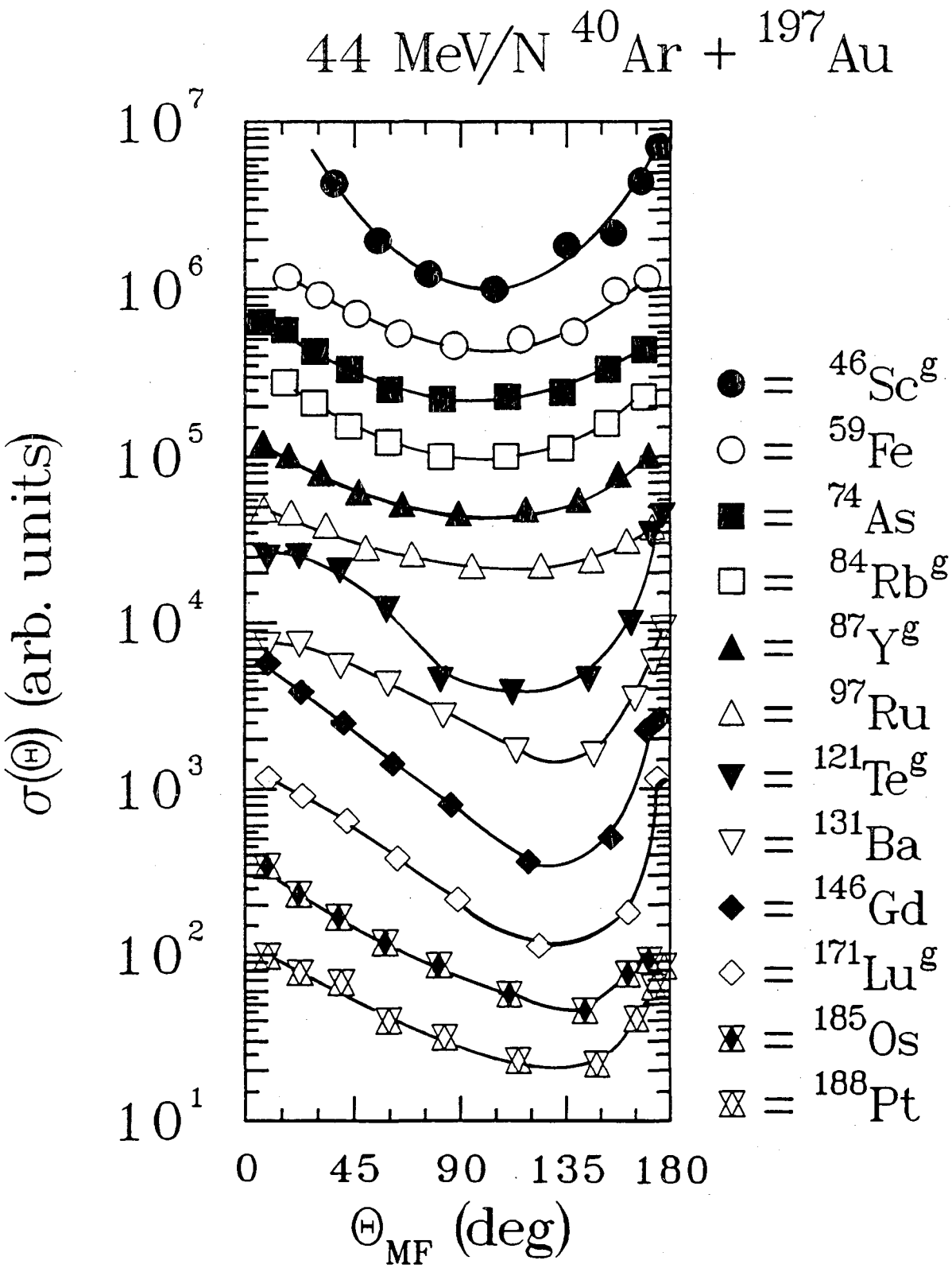

LAWRENCE BERKELEY LABORATORY
UNIVERSITY OF CALIFORNIA
INFORMATION RESOURCES DEPARTMENT
1 CYCLOTRON ROAD
BERKELEY, CALIFORNIA 94720